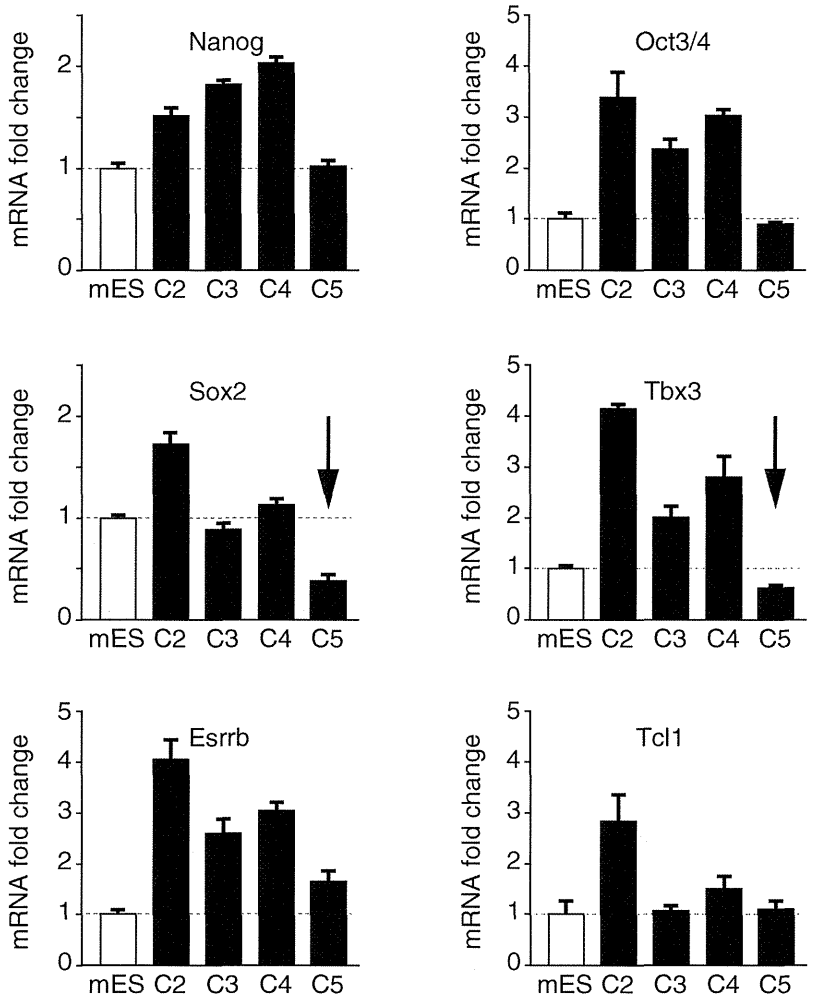

Fig.5. mRNA level of stem cell-specific genes detected by qRT–PCR analysis. Nanog, Oct3/4, Sox2, Tbx3, Esrrb, and Tcl1 were detected. The white column is the level of ES cells, and black columns are the levels of established iPS clones. The measurement of clones 2 to 5 (C2–C5) was calibrated by that of mouse ES cells and actin. In clone 5, the expression of pluripotency marker was lower when compared with other clones.

To verify the reduced reporter activity in established iPS clones, we determined the messenger RNA (mRNA) levels using quantitative real-time PCR (qRT–PCR). Expression data were corrected against the expression level of endogenous actin. The results are shown in Fig. 4F. The expression level of the MetLuc–copGFP–Neo^r cassette decreased by approximately 1:300 to 1:1000 in our established iPS cell lines when compared with that of control cells. Furthermore, clone 5 did not show any significant difference when compared with parental control MEFs, which is consistent with the results of the luciferase activity measurements.

In addition to the mRNA level, we determined the expression of the MetLuc–copGFP–Neo^r cassette in our established iPS cell lines at the protein level. As expected from the results in the previous section, we detected expression of the Neo^r protein at a molecular weight of 29 kDa in parental MEFs, which express the MetLuc–copGFP–Neo^r cassette (positive control), and in clone 5, but not in the rest of our established iPS cell lines (Fig. 4B). Furthermore, we could not detect any specific signal in the high-molecular-weight area, which suggests that efficient protein cleavage at the 2A peptide had occurred in the initially translated protein. This is in agreement with the results reported by Kim and coworkers [23].

As a final step, we detected stable transmission of the MetLuc–copGFP–Neo^r reporter cassette during multiple passages of iPS cells. The integration of the reporter cassette from passage 6 to passage 11 was confirmed with genomic PCR amplification. The MEFs immortalized with E6/E7 did not show any amplification product (lane 2 in Supplementary Fig. 2, negative control), and all of the established iPS clones showed stable amplification at passages 6 and 11. From these data, we conclude that the MetLuc–copGFP–Neo^r cassette was silenced during the reprogramming process of iPS cells (clones 2–4), but not in clone 5.

iPS cell line clone 5 showed lower expression of Sox2 and Tbx3

We tried to detect the biological difference among the established iPS clones: how biologically different between clones 2 to 4 and clone 5, which showed the different status of the silencing of the MetLuc reporter cassette? To answer this question, we first evaluated the expression level of STEMCCA–loxP reprogramming cassette. As we showed in Fig. 1D, the STEMCCA–loxP reprogramming cassette is driven by the EF1α promoter, which is resistant to the promoter silencing. As we expected, the expression level of the STEMCCA–loxP reprogramming cassette did not show any difference among each iPS clone (Fig. 4G). To elucidate the biological difference of clones 2 to 4 and clone 5, we compared gene expression of multiple markers, which associated tightly with pluripotency

(Fig. 5). Of note, the expression level of Sox2 and Tbx3 in clone 5 was lower than that in ES cells (40–60%, arrows in Fig. 5) and that in clones 2 to 4. Furthermore, the expression level of Nanog, Oct3/4, and Esrrb in clone 5 was lower than that of clones 2 to 4. From these results, we conclude that silencing status of the retrovirus promoter is a good indicator for evaluating the quality of iPS cells.

Discussion

This study demonstrated that our established reporter system containing three marker proteins—secreted-type luciferase (MetLuc), green fluorescent protein (copGFP), and a drug-resistant protein (Neo^r) bridged by self-cleavage peptides—is useful for monitoring gene silencing in iPS cells. We confirmed expression changes in three different indicators of expression of the reporters, mRNA, and protein. These results indicate that our established reporter system enables us to monitor the expression level of the exogenous reporter gene efficiently and simply from conditioned cultured medium.

In this study, we used the STEMCCA–loxP lentivirus to induce the differentiation of iPS cells. In this lentivirus, Sommer and coworkers removed the STEMCCA expression cassette by homologous recombination mediated by the Cre recombinase and loxP sequences located at the 5′ and 3′ LTR region [24]. If we were to introduce the Cre recombinase to the iPS cells, the recombination of Cre and loxP sequences would result in the removal of all four reprogramming factors. The STEMCCA–loxP lentivirus contains the EF1α promoter, which is highly resistant to silencing even in stem cells [25,26]. This promoter remains active and drives the four reprogramming factors even after iPS transformation.

In our established four iPS cell lines, clones 2 to 4 showed significant reductions in reporter activity at an early passage number (Fig. 4A). We also observed high expression of several pluripotent markers by immunostaining and qRT–PCR, indicating that genomic reprogramming in clones 2 to 4 was successful (Figs. 3 and 5). We conclude that the reduced luciferase activity was caused by gene silencing of the LTR promoter driving the MetLuc–copGFP–Neo^r expression cassette. On the other hand, clone 5 did not show any reduction in luciferase activity even at later passage numbers (>10; data not shown). The detection of mRNA derived from the MetLuc–copGFP–Neo^r expression cassette further confirms the activated status of the reporter cassette. The MetLuc–copGFP–Neo^r expression cassette did not undergo silencing, possibly because of incomplete reprogramming. As supporting evidence, the expression level of Tbx3 and Sox2 is apparently lower than that of ES cells and other clones (arrows in Fig. 5), suggesting the biological difference between clone 5 and other clones.

In addition to retroviral silencing, high-quality iPS cells are known to activate expression driven by the early transposon (ETn) promoter [27]. A combination of EOS (ETn promoter and Oct4 and Sox2 enhancers) and our developed MetLuc–copGFP–Neo^r expression cassette might enable us to select high-quality iPS cells more effectively.

Acknowledgments

We thank Gustavo Mostoslavsky (Boston University School of Medicine) for providing the STEMCCA–loxP lentiviral vector. We also thank Akane Inagaki and Shizu Hidema (Graduate School of Agricultural Science, Tohoku University) for their helpful discussions. This work was supported by research grants from the Urakami Foundation, Daiwa Securities Health Foundation, and Asahi Group Foundation as well as a Japan Society for the Promotion of Science (JSPS) grant (KAKENHI, 23650587).

Appendix A. Supplementary data

Supplementary data associated with this article can be found, in the online version, at http://dx.doi.org/10.1016/j.ab.2013.08.014.

References

[1] K. Takahashi, S. Yamanaka, Induction of pluripotent stem cells from mouse embryonic and adult fibroblast cultures by defined factors, Cell 126 (2006) 663–676.
[2] K. Okita, T. Ichisaka, S. Yamanaka, Generation of germline-competent induced pluripotent stem cells, Nature 448 (2007) 313–317.
[3] M. Wernig, A. Meissner, R. Foreman, T. Brambrink, M. Ku, K. Hochedlinger, B.E. Bernstein, R. Jaenisch, In vitro reprogramming of fibroblasts into a pluripotent ES-cell-like state, Nature 448 (2007) 318–324.
[4] N. Maherali, R. Sridharan, W. Xie, J. Utikal, S. Eminli, K. Arnold, M. Stadtfeld, R. Yachechko, J. Tchieu, R. Jaenisch, K. Plath, K. Hochedlinger, Directly reprogrammed fibroblasts show global epigenetic remodeling and widespread tissue contribution, Cell Stem Cell 1 (2007) 55–70.
[5] T. Brambrink, R. Foreman, G.G. Welstead, C.J. Lengner, M. Wernig, H. Suh, R. Jaenisch, Sequential expression of pluripotency markers during direct reprogramming of mouse somatic cells, Cell Stem Cell 2 (2008) 151–159.
[6] J. Kim, J. Chu, X. Shen, J. Wang, S.H. Orkin, An extended transcriptional network for pluripotency of embryonic stem cells, Cell 132 (2008) 1049–1061.
[7] X. Chen, H. Xu, P. Yuan, F. Fang, M. Huss, V.B. Vega, E. Wong, Y.L. Orlov, W. Zhang, J. Jiang, Y.H. Loh, H.C. Yeo, Z.X. Yeo, V. Narang, K.R. Govindarajan, B. Leong, A. Shahab, Y. Ruan, G. Bourque, W.K. Sung, N.D. Clarke, C.L. Wei, H.H. Ng, Integration of external signaling pathways with the core transcriptional network in embryonic stem cells, Cell 133 (2008) 1106–1117.
[8] R. Sridharan, J. Tchieu, M.J. Mason, R. Yachechko, E. Kuoy, S. Horvath, Q. Zhou, K. Plath, Role of the murine reprogramming factors in the induction of pluripotency, Cell 136 (2009) 364–377.
[9] T.S. Mikkelsen, J. Hanna, X. Zhang, M. Ku, M. Wernig, P. Schorderet, B.E. Bernstein, R. Jaenisch, E.S. Lander, A. Meissner, Dissecting direct reprogramming through integrative genomic analysis, Nature 454 (2008) 49–55.
[10] Z.D. Smith, I. Nachman, A. Regev, A. Meissner, Dynamic single-cell imaging of direct reprogramming reveals an early specifying event, Nat. Biotechnol. 28 (2010) 521–526.
[11] R.P. Koche, Z.D. Smith, M. Adli, H. Gu, M. Ku, A. Gnirke, B.E. Bernstein, A. Meissner, Reprogramming factor expression initiates widespread targeted chromatin remodeling, Cell Stem Cell 8 (2011) 96–105.
[12] R. Araki, Y. Jincho, Y. Hoki, M. Nakamura, C. Tamura, S. Ando, Y. Kasama, M. Abe, Conversion of ancestral fibroblasts to induced pluripotent stem cells, Stem Cells 28 (2010) 213–220.
[13] M.G. Guenther, G.M. Frampton, F. Soldner, D. Hockemeyer, M. Mitalipova, R. Jaenisch, R.A. Young, Chromatin structure and gene expression programs of human embryonic and induced pluripotent stem cells, Cell Stem Cell 7 (2010) 249–257.
[14] A.M. Newman, J.B. Cooper, Lab-specific gene expression signatures in pluripotent stem cells, Cell Stem Cell 7 (2010) 258–262.
[15] V. Ramos-Mejia, M. Munoz-Lopez, J.L. Garcia-Perez, P. Menendez, IPSC lines that do not silence the expression of the ectopic reprogramming factors may display enhanced propensity to genomic instability, Cell Res. 20 (2010) 1092–1095.
[16] M. Okada, Y. Yoneda, The timing of retroviral silencing correlates with the quality of induced pluripotent stem cell lines, Biochim. Biophys. Acta 2011 (1810) 226–235.
[17] S.V. Markova, S. Golz, L.A. Frank, B. Kalthof, E.S. Vysotski, Cloning and expression of cDNA for a luciferase from the marine copepod *Metridia longa*: a novel secreted bioluminescent reporter enzyme, J. Biol. Chem. 279 (2004) 3212–3217.
[18] T. Kitamura, Y. Koshino, F. Shibata, T. Oki, H. Nakajima, T. Nosaka, H. Kumagai, Retrovirus-mediated gene transfer and expression cloning: powerful tools in functional genomics, Exp. Hematol. 31 (2003) 1007–1014.
[19] C.A. Sommer, M. Stadtfeld, G.J. Murphy, K. Hochedlinger, D.N. Kotton, G. Mostoslavsky, Induced pluripotent stem cell generation using a single lentiviral stem cell cassette, Stem Cells 27 (2009) 543–549.
[20] Q.L. Ying, J. Wray, J. Nichols, L. Batlle-Morera, B. Doble, J. Woodgett, P. Cohen, A. Smith, The ground state of embryonic stem cell self-renewal, Nature 453 (2008) 519–523.
[21] K. Takahashi, K. Tanabe, M. Ohnuki, M. Narita, T. Ichisaka, K. Tomoda, S. Yamanaka, Induction of pluripotent stem cells from adult human fibroblasts by defined factors, Cell 131 (2007) 861–872.
[22] A. Yamamoto, S. Kumakura, M. Uchida, J.C. Barrett, T. Tsutsui, Immortalization of normal human embryonic fibroblasts by introduction of either the human papillomavirus type 16 E6 or E7 gene alone, Int. J. Cancer 106 (2003) 301–309.
[23] J.H. Kim, S.R. Lee, L.H. Li, H.J. Park, J.H. Park, K.Y. Lee, M.K. Kim, B.A. Shin, S.Y. Choi, High cleavage efficiency of a 2A peptide derived from porcine teschovirus-1 in human cell lines, zebrafish, and mice, PLoS One 6 (2011) e18556.

[24] C.A. Sommer, A.G. Sommer, T.A. Longmire, C. Christodoulou, D.D. Thomas, M. Gostissa, F.W. Alt, G.J. Murphy, D.N. Kotton, G. Mostoslavsky, Excision of reprogramming transgenes improves the differentiation potential of iPS cells generated with a single excisable vector. Stem Cells 28 (2010) 64–74.
[25] S. Hong, D.Y. Hwang, S. Yoon, O. Isacson, A. Ramezani, R.G. Hawley, K.S. Kim, Functional analysis of various promoters in lentiviral vectors at different stages of in vitro differentiation of mouse embryonic stem cells, Mol. Ther. 15 (2007) 1630–1639.
[26] J. Liu, K.L. Jones, H. Sumer, P.J. Verma, Stable transgene expression in human embryonic stem cells after simple chemical transfection, Mol. Reprod. Dev. 76 (2009) 580–586.
[27] A. Hotta, A.Y.L. Cheung, N. Farra, K. Vijayaragavan, C.A. Seguin, J.S. Draper, P. Pasceri, I.A. Maksakova, D.L. Mager, J. Rossant, M. Bhatia, J. Ellis, Isolation of human iPS cells using EOS lentiviral vectors to select for pluripotency, Nat. Methods 6 (2009) 370–378.

生体の科学　65(2):154-158, 2014

特集　細胞の少数性と多様性に挑む—シングルセルアナリシス
C．シングルセルアナリシスで見えること

単細胞技術に基づくiPS細胞の標準化

山根順子　丸山徹　藤渕航

これまでの生物学の常識を大きく覆した人工多能性幹細胞(iPS細胞；induced pluripotent stem cell)の発見がなされたのが2006年のことである[1]。iPS細胞はES細胞と異なり作製段階にヒト胚を破壊する必要がないことから，ES細胞を用いた研究において大きな障壁となっていた倫理問題が生じず，再生医療を一気に加速させる夢の細胞として登場した。体細胞にわずか数因子を導入するのみで多能性を持った細胞を生み出すことができるという報告はあまりにセンセーショナルであり，それ以降様々な細胞種由来のiPS細胞の樹立や，より安全かつ効率的な樹立法が次々に見いだされた。また，iPS細胞を用いた幹細胞生物学としての基礎研究や再生医療，創薬へ向けた応用研究など，多数の報告がなされている。世界中で樹立が試みられ報告されているiPS細胞は，樹立された数だけ質の異なる細胞になっている可能性が指摘され，今度は質の良いiPS細胞を選別する手法を開発するという新たな研究の方向性も生まれた。

iPS細胞は通常コロニー(細胞集団)として維持培養される。しかしながら，コロニーのなかでも均一な状態ではなく細胞の個性があることがわかっており，集団レベルでiPS細胞の解析を続けていくだけでは標準化を目指すことは難しい。そこでわれわれはより解像度を上げた解析が必要になると考え，従来のような“細胞集団”として遺伝子発現レベルを調べるのではなく，“個”としての細胞，つまり“シングルセルレベル”での遺伝子発現を調べ，標準化に向けた試みを行った。

Ⅰ．シングルセルトランスクリプトーム解析

2009年にTangら[2]によってシングルセルレベルでRNA-seqを行う方法が発表されてから，これまでに幾つかの手法が報告されてきた。われわれが行ったシングルセルトランスクリプトーム解析の手法は各細胞を判別するためのDNAバーコードをtemplate switchingにより導入するSTRT法[3]であり，同時に大量のシングルセルを解析できる利点がある。この方法では，mRNAの5'末端にDNAバーコードを導入するため，次世代シークエンサーで読まれたリードは5'末端側の配列であるという特徴がある。その他の手法で最近報告されたものでは，SMART-seq[4]やCEL-seq[5]，Quartz-seq[6]などがあり，そのうちCEL-seq，Quartz-seqは3'末端側のバイアスがあることが知られている。加えて，これまで問題とされてきたデータの精度についても，Quartz-seqでは細胞周期が区別できるまで改善されており，この先シングルセルトランスクリプトーム解析が大幅に普及することが予想される。

Standardization of iPS cells by single-cell transcriptome analysis

Yamane Junko：京都大学iPS細胞研究所(特定研究員：〒606-8507 京都市左京区聖護院川原町53)
Maruyama Toru：早稲田大学大学院 先進理工学研究科 生命医科学専攻(修士課程)，京都大学iPS細胞研究所(特別研究学生)
Fujibuchi Wataru：京都大学iPS細胞研究所(教授)

0370-9531/04/¥500/論文/JCOPY

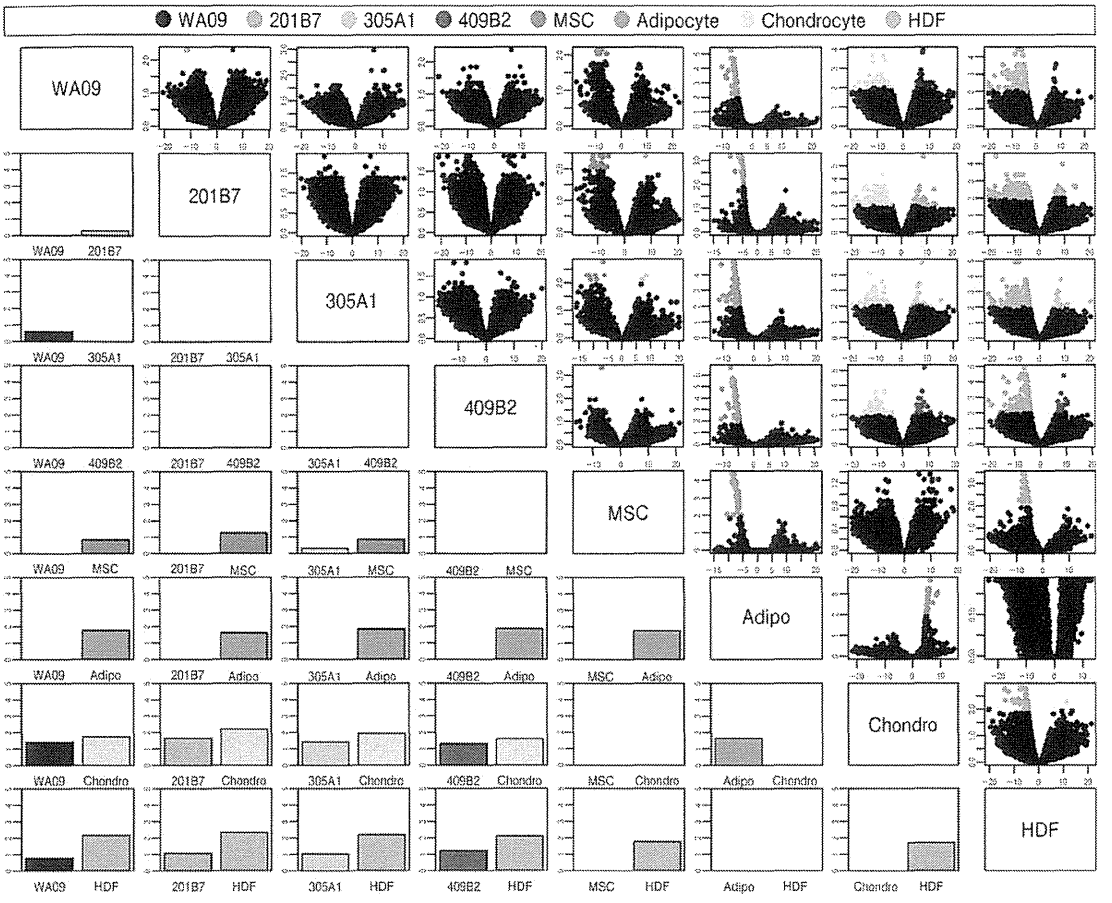

図1　DEG解析

対角線より上：Volcano plot(横軸：$\log_2$(FC)，縦軸：$\log_{10}$(FDR))，色がついたプロットは有意差(FDR<0.01)があった遺伝子。対角線より下：DEGの数を示す棒グラフ。プロット・棒の色は細胞種に対応している。例えば赤いプロットはAdipocyteで発現が高い遺伝子を，赤い棒はAdipocyteで発現が高い遺伝子の数を表す。

Ⅱ．シングルセルトランスクリプトーム解析により見えてきた特徴

われわれは異なる手法によって樹立されたiPS細胞3種類(201B7，305A1，409B2)に加えてES細胞1種類(WA09)，ヒトの体細胞4種類(MSC：間葉系幹細胞，Chondro：軟骨細胞，adipo(誘導させた)脂肪細胞，HDF：皮膚線維芽細胞)の計8細胞種を対象にしてシングルセルレベルのトランスクリプトーム解析を行った。

まず，Bioconductorのedge Rパッケージを用いて2細胞種間で真の発現変動遺伝子(DEG)の数を調べたところ，ES細胞とiPS細胞間で発現変動がある遺伝子はほとんど見つからなかった(図1)。しかし，本解析は細胞集団を対象にした手法を適用しているので，シングルセルレベルでの解析とは結果が異なる可能性がある。

そこでシングルセルレベルでの各種細胞における遺伝子発現パターンの特徴をより詳細に調べるため，8細胞種の主成分分析(PCA)を行ったところ，おおよそ細胞種ごとにクラスターを形成していることが確認できた(図2)。この結果から軟骨細胞とHDFのクラスターが重なっていることがわかったが，これらの細胞種間では遷移が起こることが知られている[7]。よって，単一細胞のトランスクリプトームには細胞系譜における細胞間の関係性や，細胞間で遷移が起こりうる可能性といった新たな情報が包含されている可能性が示唆

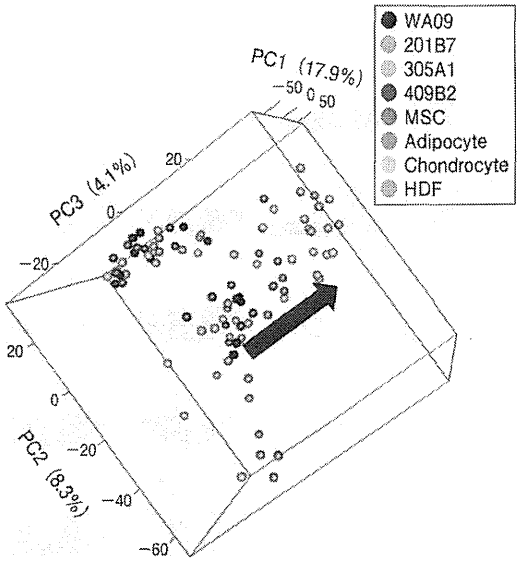

図2　8細胞種の主成分解析(PCA)
細胞ごとにある程度クラスターができている。括弧内は各種成分の寄与率を示す。HDFとChondrocyteが混在しているが，これはHDFとChondrocyteの間でトランジションが起こりやすいことを示唆していると考えられる。また，矢印の方向に相転移が起こりうることを示唆している。

された。これまでの集団として解析してきた方法では平均化されてしまい見えていなかった細胞本来のばらつきの様相の一端が明らかになった。

また，遺伝子発現の揺らぎの大きさを評価するために，細胞種ごとに全遺伝子の変動係数(CV)を調べた(図3)。細胞集団での解析と一致して，すべての細胞でハウスキーピング遺伝子のCVは他の遺伝子と比較して遺伝子発現の揺らぎが小さいという結果が得られた。微量なサンプルを対象とするシングルセル解析を行ううえで，得られた結果が細胞由来の揺らぎによるものか，テクニカルな問題により生じる差を見ているのかを見極めることは非常に重要である。よって，指標の一つとなるハウスキーピング遺伝子の発現の揺らぎが他の遺伝子と比べて小さいという結果はシングルセルを扱う研究を進めるにあたり精度の良さを確認するための大きな情報となり得る。

最後に，全遺伝子の変動係数の解析において今回調べた細胞間でヒストグラム分布の異なる遺伝子について一部報告する。まず，DNAメチル化にかかわるDNMT3Bは既報のように[8]，ES細胞，iPS細胞の多能性幹細胞群ではほぼ共通し発現レ

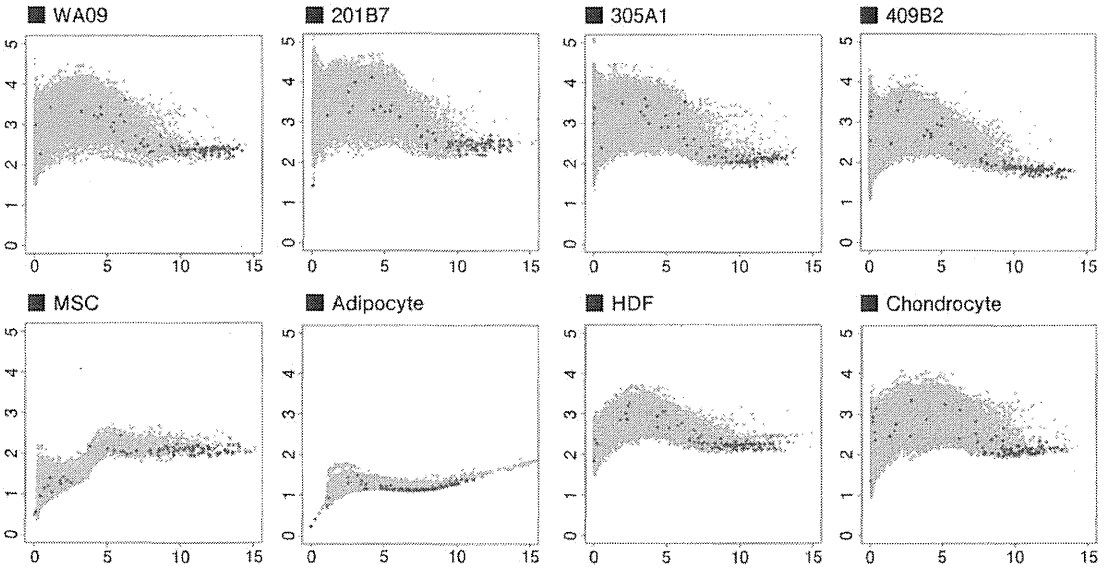

図3　全遺伝子の変動係数(CV)
各点は遺伝子に対応しており，赤点はハウスキーピング遺伝子に対応している。横軸は$\log_2$(RPM)の平均，縦軸はedgeRによって算出した発現の変動(biological coefficient of variation)を表している。下に位置する遺伝子ほど安定に発現していることを意味する。

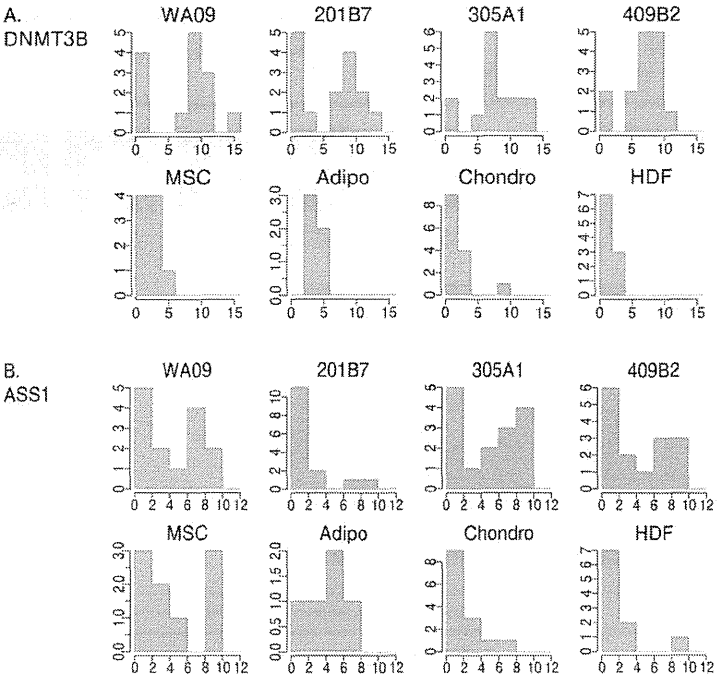

図 4　ヒストグラムの分布で差が見られた遺伝子例（横軸は $\log_2$(RPM+1)）
A. は多能性幹細胞と分化細胞の間で顕著な差が見られた。B. は多能性幹細胞の中の比較で一部の株(201B7)で異なる分布が見られた。

ベルの高い分布が見られ，逆に分化細胞ではいずれも発現レベルの低い分布が傾向として見られた(図 4A)。また，アルギニン生合成経路にかかわる酵素の一つである ASS1 は多能性幹細胞群の中で比較をした場合，201B7 株でのみ低発現の分布を示している傾向があった。この遺伝子は分化細胞でも比較的低発現の分布を示している(図 4B)。このように平均で解析していると見えてこなかった遺伝子発現の分布が，個々のレベルで見ると差が見えてくるケースがある。

以上のように，われわれはシングルセルトランスクリプトーム解析によって，これまでの細胞集団を対象にする解析では見えなかった事象を確認することができた。

おわりに

シングルセル RNA-seq 解析が普及するに伴い，これまで 250 種類程度と言われてきた細胞がより細かく分類されるようになる可能性がある。そこで，われわれの研究室では細胞のデータベースである“SHOGoiN”を開発しており，細胞の遺伝子発現プロファイル，画像，形態計測情報，実験条件などのメタデータ，文献情報を貯蔵している(図 5)。ユーザーはウェブブラウザを通して本データベースにアクセスし，細胞に関する情報を検索することができる。

今後，われわれはシングルセル RNA-seq 解析と体系的に貯蔵された細胞のデータを用いて，細胞に普遍的に存在する理論を見つけることを目指している。その一つとして次のような問題に取り組んでいる。

iPS 細胞を作製する際には，元となる体細胞に *Oct4*, *Sox2*, *Klf4*, *c-Myc* などの遺伝子を導入し，強制的に発現させる必要がある。しかし，すべての細胞に同じ刺激を与えているにもかかわらず，なぜ iPS 細胞の作製効率は悪く，質の良し悪しがあるのだろうか。われわれはこの問題に対して以下のようなモデルを考えている。遺伝子の発現は同じ種類の細胞であっても均一でなく，揺らぎがある。揺らぎは転写因子の結合や転写反応，

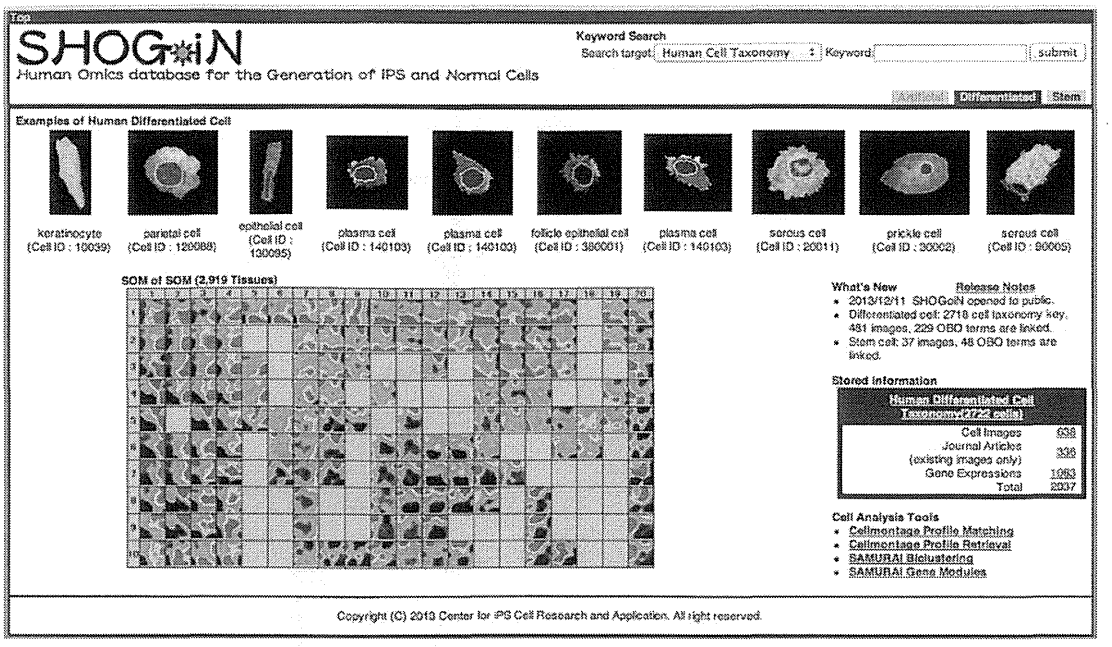

図5　ヒト細胞情報統合データベース“SHOGoiN”
http://shogoindb.cira.kyoto-u.ac.jp

RNAの分解といったイベントが確率的であることに起因している[9]。Huangらの論文[10]にもあるように，われわれはこういった遺伝子発現の揺らぎが細胞状態の変化に影響を与えているため，細胞分化やiPS細胞の作製が確率的なものになっているのではないかと考えている。よって，揺らぎが細胞分化に与える影響を解き明かすことができれば，質の良い細胞をより効率的に作製する手法が明らかになるかもしれない。また，シングルセル解析により得られた詳細な情報をデータベースに集約し，広く研究者らが利用することで，iPS細胞の標準化や，そこから分化させた各種分化細胞の標準化に向けた足がかりとなることを期待している。

謝辞　本研究は『内閣府最先端研究開発支援プログラム（FIRSTプログラム）』の支援のもと行いました。

●文　献

1) Takahashi K, Yamanaka S：*Cell* **126**：663-676, 2006
2) Tang F, Barbacioru C, Wang Y et al：*Nat Methods* **6**：377-382, 2009
3) Islam S, Kjällquist U, Moliner A et al：*Genome Res* **21**：1160-1167, 2011
4) Ramsköld D, Luo S, Wang Y-C et al：*Nat Biotech* **30**：777-782, 2012
5) Hashimshony T, Wagner F, Sher N et al：*Cell Rep* **2**：666-673, 2012
6) Sasagawa Y, Nikaido I, Hayashi T et al：*Genome Biol* **14**：R31, 2013
7) Outani H, Okada M, Yamashita A et al：*ProS One* **8**：e77365, 2013
8) Takahashi K, Tanabe K, Ohnuki M et al：*Cell* **131**：861-872, 2007
9) Wills QF, Livak KJ, Tipping AJ et al：*Nat Biotechnol* **31**：748-752, 2013
10) Chang HH, Hemberg M, Barahona M et al：*Nature* **453**：544-547, 2008

OPEN ACCESS Freely available online

PLOS ONE

Commensal Microbiota Contributes to Chronic Endocarditis in *TAX1BP1* Deficient Mice

Satoko Nakano[1,2], Emi Ikebe[1], Yoshiyuki Tsukamoto[3], Yan Wang[4], Takashi Matsumoto[1], Takahiro Mitsui[1], Takaaki Yahiro[1], Kunimitsu Inoue[1], Hiroaki Kawazato[5], Aiko Yasuda[5], Kanako Ito[6], Shigeo Yokoyama[7], Naohiko Takahashi[8], Mitsuo Hori[9], Tatsuo Shimada[10], Masatsugu Moriyama[3], Toshiaki Kubota[2], Katsushige Ono[4], Wataru Fujibuchi[11], Kuan-Teh Jeang[12], Hidekatsu Iha[1]*, Akira Nishizono[1]

1 Department of Microbiology, Faculty of Medicine, Oita University, Yufu, Oita, Japan, **2** Department of Ophthalmology, Faculty of Medicine, Oita University, Yufu, Oita, Japan, **3** Department of Molecular Pathology, Faculty of Medicine, Oita University, Yufu, Oita, Japan, **4** Department of Pathophysiology, Faculty of Medicine, Oita University, Yufu, Oita, Japan, **5** Research Promotion Institute, Faculty of Medicine, Oita University, Yufu, Oita, Japan, **6** Department of Internal Medicine II, Faculty of Medicine, Oita University, Yufu, Oita, Japan, **7** Department of Diagnostic Pathology, Faculty of Medicine, Oita University, Yufu, Oita, Japan, **8** Department of Laboratory Examination and Diagnostics, Faculty of Medicine, Oita University, Yufu, Oita, Japan, **9** Division of Hematology, Ibaragi Prefectural Central Hospital, Kasama, Ibaragi, Japan, **10** Department of Health Science, Oita University School of Nursing, Yufu, Oita, Japan, **11** Department of Cell Growth and Differentiation, Center for iPS Cell Research and Application, Kyoto University, Kyoto, Japan, **12** Laboratory of Molecular Microbiology, National Institute of Allergy and Infectious Diseases, National Institutes of Health, Bethesda, Maryland, United States of America

Abstract

Tax1-binding protein 1 (Tax1bp1) negatively regulates NF-κB by editing the ubiquitylation of target molecules by its catalytic partner A20. Genetically engineered *TAX1BP1*-deficient (KO) mice develop age-dependent inflammatory constitutions in multiple organs manifested as valvulitis or dermatitis and succumb to premature death. Laser capture dissection and gene expression microarray analysis on the mitral valves of *TAX1BP1*-KO mice (8 and 16 week old) revealed 588 gene transcription alterations from the wild type. *SAA3* (serum amyloid A3), *CHI3L1*, *HP*, *IL1B* and *SPP1/OPN* were induced 1,180-, 361-, 187-, 122- and 101-fold respectively. *WIF1* (Wnt inhibitory factor 1) exhibited 11-fold reduction. Intense Saa3 staining and significant I-κBα reduction were reconfirmed and massive infiltration of inflammatory lymphocytes and edema formation were seen in the area. Antibiotics-induced 'germ free' status or the additional *MyD88* deficiency significantly ameliorated *TAX1BP1*-KO mice's inflammatory lesions. These pathological conditions, as we named 'pseudo-infective endocarditis' were boosted by the commensal microbiota who are usually harmless by their nature. This experimental outcome raises a novel mechanistic linkage between endothelial inflammation caused by the ubiquitin remodeling immune regulators and fatal cardiac dysfunction.

Citation: Nakano S, Ikebe E, Tsukamoto Y, Wang Y, Matsumoto T, et al. (2013) Commensal Microbiota Contributes to Chronic Endocarditis in *TAX1BP1* Deficient Mice. PLoS ONE 8(9): e73205. doi:10.1371/journal.pone.0073205

Editor: Dong-Yan Jin, University of Hong Kong, Hong Kong

Received May 10, 2013; **Accepted** July 17, 2013; **Published** September 27, 2013

Funding: This study is supported in part by grants from the Ministry of Education, Culture, Sports, Science, and Technology; Okinawa Science and Technology Promotion Center (OSTPC); Miyazaki Prefectural Industrial Support Foundation. E.I. is a research fellow of the OSTPC and was a recipient of the Hita Tenryosui Research Scholarship from Hita Tenryosui Co. Ltd. The funders had no role in study design, data collection and analysis, decision to publish, or preparation of the manuscript.

Competing Interests: The authors have read the journal's policy and have the following conflicts: E.I. is a research fellow of the Okinawa Science and Technology Promotion Center and was a recipient of the Hita Tenryosui Research Scholarship from Hita Tenryosui Co. Ltd. There are no patents, products in development or marketed products to declare. This does not alter the authors' adherence to all the PLOS ONE policies on sharing data and materials.

* E-mail: hiha@oita-u.ac.jp

Introduction

The transcription factor NF-κB is essential for the regulation of the innate and adaptive immune responses. NF-κB is activated in response to a wide variety of stimuli, such as inflammation, DNA damage, or nociception [1,2], and is involved in embryogenesis and multiple tissue development [3]. The NF-κB family comprises five proteins including RelA (p65), RelB, c-Rel, NF-κB1, and NF-κB2, and their transcriptional activities are tightly controlled to ensure their transient signaling in response to specific stimuli. The NF-κB signaling cascade is usually triggered by sensor molecules, such as toll-like receptor (TLR) family proteins. These proteins can identify the presence of a wide range of microorganisms and then transmit that information through phosphorylation relays to downstream kinases, which eventually culminate at the I-κB kinase (IKK). IKK activates NF-κB via phosphorylation of inhibitory I-κB proteins (primarily I-κBα), which leads to its ubiquitylation and degradation by the 26S proteasome complex and allows NF-κB to enter the nucleus. I-κB is induced by NF-κB to function in a negative feedback loop that terminates NF-κB signaling. Aberrant activation of NF-κB has been linked to several pathological features such as allergic responses, autoimmune diseases, septic shock, and carcinogenesis in a variety of organs [4].

In addition to I-κB, deubiquitinase A20 (also referred to as TNFα-induced protein 3 or TNFAIP3) targets important signaling intermediates upstream of I-κB to terminate NF-κB activation [5,6]. A20 cleaves Lys63 (K63)-linked polyubiquitin chains on

overlapping substrates, such as E3 ubiquitin ligase TRAF6 and adaptor molecule RIP1, with the help of the substrate-specific adaptor Tax1-binding protein 1 (Tax1bp1 [7,8]). Tax1bp1 intrinsically regulates NF-κB by recruiting A20 to the target molecules to remove their polyubiquitin chains, which play important roles in their assembly into the IKK complex [8,9]. Deficiencies in A20 or Tax1bp1 lead to uncontrolled and spontaneous systemic inflammation in mice as a result of unchecked NF-κB signaling [8,10].

Tax1bp1 was originally identified as a host cell factor that binds to the encoded protein of human T-lymphotropic virus type 1 (HTLV-1), known as Tax1 [7]. Tax1 is a potent activator of NF-κB and a major pathogenic factor in HTLV-1 associated diseases (HAD), such as HTLV-1 associated myelopathy (HAM) or HTLV-1 uveitis (HU [11]), and adult T-cell leukemia (ATL [12]). Tax1 interrupts the ability of Tax1bp1 to connect to and recruit A20 to target molecules and thus evokes persistent NF-κB activation [13,14]. Tax1 also activates NF-κB by binding to the NF-κB essential modulator (NEMO), a regulatory subunit of IKK [15]. The aberrant activation of NF-κB in HADs can therefore be attributed to Tax1, which leads to Tax1bp1 dysfunction, over-activation of IKK, or both. Epidemiological studies provide support for a close link between HTLV-1 infection and HAD or other inflammatory diseases such as Sjögren's syndrome [16], vascular dementia [17], and atherosclerosis [18]. Moreover, recent accumulating evidence strongly suggests that several mutations in the *A20* locus are primarily responsible for the development of Crohn's disease, rheumatoid arthritis, systemic lupus erythematosus, psoriasis and type 1 diabetes [19].

For research purposes, we established *TAX1BP1*-deficient (-KO) mice, which display exacerbation of inflammation (characterized as valvulitis and dermatitis) in an age-dependent manner in addition to functional inadequacies manifested in growth retardation and premature death [8]. To elucidate the molecular mechanisms underlying the manifestation of inflammatory symptoms and their link to premature or possible cardiac abnormalities induced by *TAX1BP1*-deficiency, we performed a series of pathological evaluations using *TAX1BP1*-KO mice: (1) laser capture microdissection (LCM)- and gene expression microarray-based profiling of the mitral valves, which was reevaluated using real-time polymerase chain reaction (RT-PCR); (2) multiplex cytokine and chemokine quantitation in sera on systemic inflammatory constitution; (3) histochemical and electron microscopic analyses of multiple pathogenic foci; and (4) antibiotic treatments and cross experimentation with *MyD88*-deficient mice [20] to examine the role of commensal microbiota in the pathogenesis of *TAX1BP1*-KO mice.

From our experimental data, we conclude that systemic inflammation and cardiac structural abnormalities in *TAX1BP1*-KO mice originated from commensal microbiota, which are usually harmless in nature. Furthermore, these results indicate a potential risk to asymptomatic HTLV-1 carriers, which should be addressed by further clinical research.

Table 1. Primer sequences.

SAA3	**acagcctctctggcatcg**	**atgctcggggaactatgat**	**#26**
TAX1BP1	ataaaaatgtgtaatagtcacgagcag	cactccaaagattgggttgg	#56
EFCAB2	tgtccgtcgtggctatgac	cctgcttcaccaccttcttg	#80
GAPDH	tcgaccatgaatcgaataataca	tgcagctctccttcagtcg	#89

doi:10.1371/journal.pone.0073205.t001

Table 2.

IL6	**gctaccaaactgga tataatcagga**	**ccaggtagctatgg tactccagaa**	**#6**
CXCL1	agactccagccacacactccaa	tgacagcgcagctcattg	#83
GAPDH	tcgaccatgaatcgaataataca	tgcagctctccttcagtcg	#89

doi:10.1371/journal.pone.0073205.t002

Materials and Methods

Animals

TAX1BP1-KO mice having replaced their exon 17 region with CMV-driven NEO gene in reverse orientation [8] and their wild-type (WT) littermates as controls were analyzed throughout the experiment. These strains are maintained as F9 or advanced generations of C57BL/6CrSlc or the original 129/+ Ter/SvJcl. *MyD88* deficient mice are kind gifts from professor Hitoshi Nakashima from Fukuoka University [21]. Homozygous *TAX1BP1*-KO mice were crossbred with homozygous *MyD88*-KO background to generate *MyD88/TAX1BP1*-KO mutants. Each of the targeted loci was evaluated by PCR. These mice were bred and maintained under specific pathogen-free (SPF) conditions at the animal facility of Oita University Faculty of Medicine. All the mice related manipulations were performed with protocols approved by the animal ethics committee at the Oita University (Justified numbers, daily care, treatment and euthanasia procedures).

Laser capture microdissection

Three mitral valves from 8 or 16 week old (-wk) male *TAX1BP1*-KO and their WT littermates were collected by Arcturus XT laser capture microdissection system according to a manufacture's directions.

RNA Isolation and gene expression microarray analysis

Total RNAs were purified from the mitral valves using RNeasy mini kit (Qiagen). RNA quantity and purity were evaluated using a NanoDrop 2000 (NanoDrop Technologies). All RNA samples were labeled, linearly amplified by Low Input Quick Amp Labeling Kit and RNA Spike-In Kit then analyzed with Whole Mouse Genome Microarray Kit (Agilent). Signal intensities were quantitated with laser confocal scanner and analyzed with Feature Extraction software (Version 10.7.3.1, Agilent) and R statistical package (Version 2.15.1). Probe set data were median-normalized per chip. Empirical Bayesian method controlling for false discovery rate (FDR: <3% and logFC >1.0 [22]) for comparison of differentially expressed between *TAX1BP1*-KO mice and their WT. Principal Component Analysis (PCA) for the systematic trend examination, heatmaps by R Software and volcano plot analysis were applied to identify the single mRNA differentially expressed in *TAX1BP1*-KO mice (log2-fold expression change on the x-axis and t test p values on the y-axis, negative log). Each dot represents a single probe. The complete gene expression dataset can be viewed in the Gene Expression Omnibus (GEO) repository accession number GSE43932 (www.ncbi.nlm.nih.gov/geo/query/acc.cgi?acc = GSE43932).

Quantitative real time-polymerase chain reaction (RT-PCR)

Taqman quantitative RT-PCR was performed to validate a subset of genes. Random hexamer-primed cDNA templates were

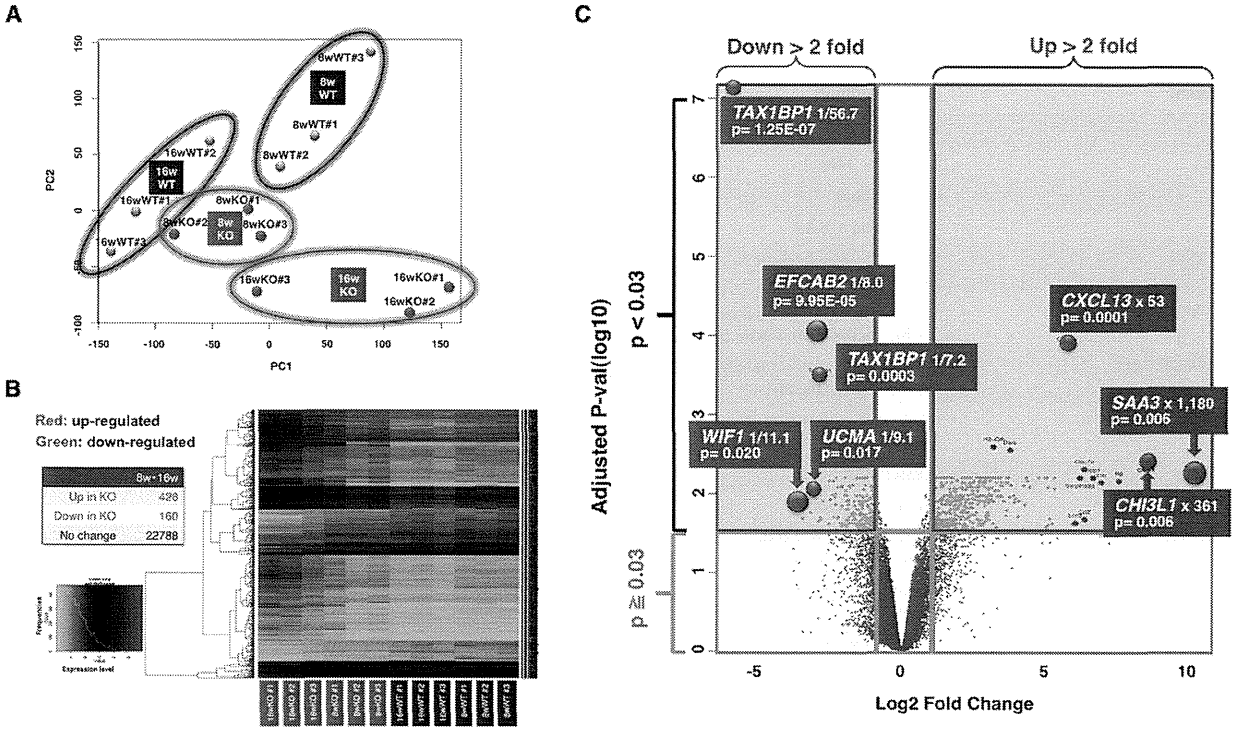

Figure 1. Elevated inflammatory profiles in the multiple organs of *TAX1BP1*-KO mice. Mitral valve tissues from either 8 or 16 week old (-wk) *TAX1BP1*-KO mice or their wild-type littermates were collected by Arcturus XT LCM system and total RNAs were prepared by RNeasy mini kit (Qiagen). Each cDNA pool was generated from the individual RNA sample and gene expression profiles were evaluated using Whole Mouse Genome Microarray Kit (Agilent). **A**) Principal component analysis (PCA) by conditions was performed on R statistical package (Version 2.15.1) and represented as a scatterplots of whole gene expression profiles of 8- or 16-wk *TAX1BP1*-KO mice (8wKO #1- #3 or 16wKO #1-#3, surrounded by red circles) and their WT littermates (8wWT #1- #3 or 16wWT #1-#3, blue circles). The PCA plot showed that samples clustered based on their genetic backgrounds. Data represent n = 12. Component % variance; PC1 = 34.95%, PC2 = 19.48%. **B**) Heat map representation of differentially expressed genes in the mitral valves from either 8- or 16-wk *TAX1BP1*-KO mice or their WT littermates. 588 genes were differentially expressed in *TAX1BP1*-KO vs. WT littermates ($P<0.03$). Each column represents the expression profile of either the *TAX1BP1*-KO mice or WT littermates. Red and green colors indicate high and low expression levels, respectively, relative to the mean (see color bar). **C**) Volcano plot analysis of microarray revealed that 588 probes were significantly expressed more than 2-fold vs control. Red and green areas indicate significant increasing and decreasing changes in gene expression ($p<0.03$).
doi:10.1371/journal.pone.0073205.g001

synthesized from purified (RNAs ReverTra Ace®, TOYOBO). The output of RT-PCR reactions were quantitated with Light-Cycler® R 480 System (Roche). Primer sequences were listed in Table 1. Each reaction was run in triplicate with endogenous control *GAPDH* on the same reaction plate.

Multiple cytokine & chemokine quantitation

The 3-, 8-, 16- and 32-wk male *TAX1BP1*-KO and their WT littermates were anesthetized and an aliquot of serum (12.5 μl) from heart blood were collected (n = 5/groups). Quantitation of 23 cytokines and chemokines was performed by a multiplex ELISA system (Bio-Plex, BioRad) and analyzed by the Bio-Plex Manager Software 6.1 (Bio-Rad) with a five-parameter curve-fitting algorithm for standard curve calculations.

Immunohistochemistry

A standard avidin-biotin-peroxidase technique or hematoxylin and eosin (HE) staining were employed for Saa3 and I-κBα staining or morphological observation of heart, liver and skin tissues of 8- or 16-wk male *TAX1BP1*-KO and their WT littermates (n = 5/groups). Rabbit polyclonal anti-Saa3 antibody (ab59736, abcum), rabbit monoclonal anti-I-κBα antibody (ab32518, abcum) or control antibody for visualization of antigens with EnVision + System-HRP Labelled Polymer Anti-Rabbit (Dako). DAB + Liquid (Dako) for positive staining and Mayer's hematoxylin solution for counterstaing. Images were captured with BZ-9000 (KEYENCE). Mice whole eye sections were examined with anti-T6BP antibody (ab22049, abcam). Anti-IgG (H+L), rabbit, goat-poly, DyLight 649 (KPL) was used as secondary antibodies.

Electron microscopy

For transmission electron microscopy (TEM), mitral valve, atrioventricular node, sinoatrial node and papillary muscles of the left ventricle of 8-, 16-, 60-wk male *TAX1BP1*-KO and their WT littermates (n = 3/groups) were fixed with 2.5% glutaraldehyde/ 2% paraformaldehyde in a 0.1 M cacodylate buffer (pH7.4) for 3 hr or longer at 4°C. After a washing in the cacodylate buffer, specimens were postfixed in 2% osmium tetroxide in cacodylate buffer for 2 hr, washed with cacodylate buffer, dehydrated with ethanol and embedded in epoxy resin. Thin section specimens (80–90 nm) were then stained with uranyl acetate and lead cystate and examined with TEM H-7650 (at 80 kV, HITACHI).

Western blotting

Tissues from liver, heart, spleen, muscle, lung, skin, stomach and brain from WT BL6 were lysed with Co-IP buffer [23] and equal amounts of protein solutions (20 μg/lane) were separated by

Table 3. Gene symbol, gene description, fold change and p-value for all genes up-regulated by >20-fold in *TAX1BP1*-KO mice.

SYMBOL	DESCRIPTION	Fold activation	adj.P. Val
SAA3	Serum amyloid A 3	1179.5	0.006
CHI3L1	Chitinase 3-like 1	361.0	0.006
HP	Haptoglobin	187.2	0.007
IL1B	Interleukin 1 beta	121.9	0.007
SPP1/OPN	Secreted phosphoprotein 1/Osteopontin	100.7	0.006
CCL2/MCP1	Chemokine (C-C motif) ligand 2/Monocyte chemotactic protein-1	81.7	0.021
CLEC7A/DECTIN1	C-type lectin domain family 7, member a/Dectin-1	81.0	0.005
SERPINA3G	Serine (or cysteine) peptidase inhibitor, clade A, member 3G	73.0	0.006
LCN2	Lipocalin 2	65.3	0.024
SAA1	Serum amyloid A 1	61.1	0.024
CXCL13/BLC	Chemokine (C-X-C motif) ligand 13/B lymphocyte chemo-attractant	52.9	0.0001
SLPI	Secretory leukocyte peptidase inhibitor	39.8	0.009
CLEC4D/DECTIN2	C-type lectin domain family 4, member d	39.6	0.006
TIMP1	Tissue inhibitor of metalloproteinase 1	37.4	0.024
CCL17/TARC	Chemokine (C-C motif) ligand 17/Thymus and activation regulated chemokine	35.2	0.020
CCL7	Chemokine (C-C motif) ligand 7	33.8	0.025
LGALS3/GALECTIN3	Lectin, galactose binding, soluble 3/Galectin-3	33.5	0.008
SIRPB1A	Signal-regulatory protein beta 1A	33.3	0.006
CHL1	Cell adhesion molecule with homology to L1CAM	32.4	0.027
CCL8	Chemokine (C-C motif) ligand 8	31.4	0.006
BCL2A1B	B-cell leukemia/lymphoma 2 related protein A1b	27.0	0.006
MEFV	Mediterranean fever	26.7	0.006
PLAC8	Placenta-specific 8	21.7	0.008
ZMYND15	Zinc finger, MYND-type containing 15	20.6	0.007
ITGAX	Integrin alpha X	20.0	0.006

Statistical significance ($p<0.03$) was calculated using the Empirical Bayesian method controlling for false discovery rate (FDR) <3% and logFC >1.0 on R statistical package (Version 2.15.1). Fold change represents a comparison between mean normalized signal intensity for control (n = 6) versus *TAX1BP1*-KO mice (n = 6).
doi:10.1371/journal.pone.0073205.t003

SDS-PAGE and transferred to immobilion membranes (Millipore) and incubated with primary antibodies, T6BP Antibody (sc-15274, Santa Cruz) or anti-Tubulin antibody (ab6160, abcum) and secondary antibodies, donkey anti-goat IgG-HRP (sc-2033, Santa Cruz) or ZyMAX^{TM} Goat anti-Rat IgG(H+L) HRP conjugate (81–9520, invitrogen) and visualized with ECL Western Blotting Detection System (GE Healthcare Lifesciences) and high-performance chemiluminescence film.

Evaluation of physiological responses to LPS-stimulation

200 μg of *Salmonella typhimurium* lipopolysaccharide (LPS, Sigma) in 100 μl sterile pyrogen-free saline were injected into the footpads of *TAX1BP1*-KO or WT littermates (n = 4/groups). Tissue lysates were prepared from eyeball and the expression of Tax1bp1, I-κBα (anti-I-κBα rabbit mAb, #4812, Cell Signaling Technology) and Tubulin were evaluated by western blotting. Total RNAs were prepared from eyeballs of *TAX1BP1*-KO or WT littermates (n = 4/groups). Taqman quantitative RT-PCR was performed as described above (See Table 2).

Sera from peripheral blood samples were collected 0, 6 and 12 hr after LPS injection and quantitated with Bio-Plex Pro^{TM} Mouse Cytokine 23-plex kit.

Enzyme-linked immunosorbant assay (ELISA)

The amounts of Saa3 and Cxcl13 Sera from 16-wk mice (n = 5/group) were measured with MOUSE SAA-3 ELISA KIT (Millipore) and Mouse CXCL13/BLC/BCA-1 Quantikine ELISA Kit (R&D Systems).

Table 4. Gene symbol, gene description, fold change and p-value for all genes down-regulated by >5 fold in *TAX1BP1*-KO mice.

SYMBOL	DESCRIPTION	Fold suppression	adj.P. Val
TAX1BP1	Tax1 (human T-cell leukemia virus type I) binding protein 1	56.7	0.0000001
WIF1	Wnt inhibitory factor 1	11.1	0.0205
UCMA	Upper zone of growth plate and cartilage matrix associated	9.1	0.0173
EFCAB2	EF-hand calcium binding domain 2	8.0	0.0001
FAM107A/DRR1	Family with sequence similarity 107, member A/down-regulated in renal cell carcinoma 1	7.6	0.0219
TSC22D3	TSC22 domain family, member 3	7.3	0.0197
TAX1BP1	Tax1 (human T-cell leukemia virus type I) binding protein 1	7.2	0.0004
MAP3K6/ASK2	Mitogen-activated protein kinase kinase kinase 6	7.1	0.0212
6030422H21RIK	RIKEN cDNA 6030422H21 gene	6.8	0.0124
TSC22D3	TSC22 domain family, member 3	5.9	0.0240
PENK	Preproenkephalin	5.7	0.0119
CNTFR	Ciliary neurotrophic factor receptor	5.3	0.0104
COL11A2	Collagen, type XI, alpha 2	5.3	0.0069
RXFP3	Relaxin family peptide receptor 3	5.2	0.0197
NRXN1	Neurexin I	5.1	0.0110
CYTL1	Cytokine-like 1	5.0	0.0099

Statistical significance ($p<0.03$) was calculated using the Empirical Bayesian method controlling for false discovery rate (FDR) <3% and logFC >1.0 on R statistical package (Version 2.15.1). Fold change represents a comparison between mean normalized signal intensity for control (n = 6) versus *TAX1BP1*-KO mice (n = 6).
doi:10.1371/journal.pone.0073205.t004

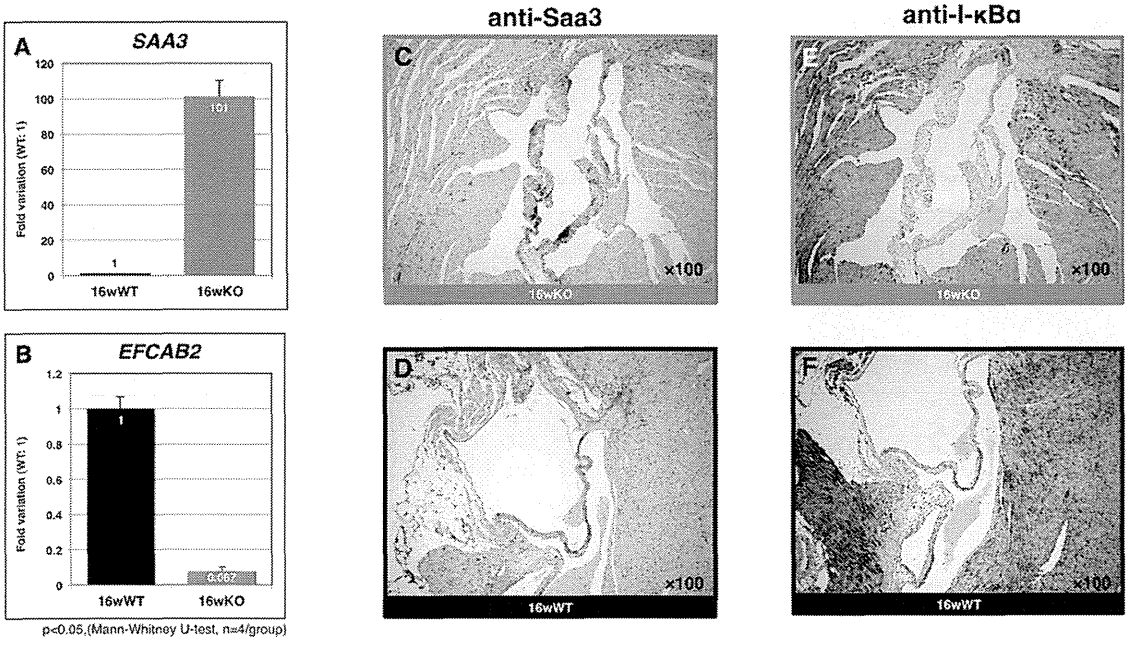

Figure 2. Validation of genes and proteins identified their expression alteration in the mitral valves of *TAX1BP1*-KO mice. RT-PCR validation of genes identified their expression alteration in the mitral valves of *TAX1BP1*-KO mice, **A**) *SAA3* **B**) *EFCAB2* respectively. Gray bar: *TAX1BP1*-KO, black bar: WT. Mitral valve specimens were prepared from 16-wk *TAX1BP1*-KO mice or their WT littermates and stained by anti-Saa3 antibody (**C** and **D**) or anti-I-κBα antibody respectively (**E** and **F**).
doi:10.1371/journal.pone.0073205.g002

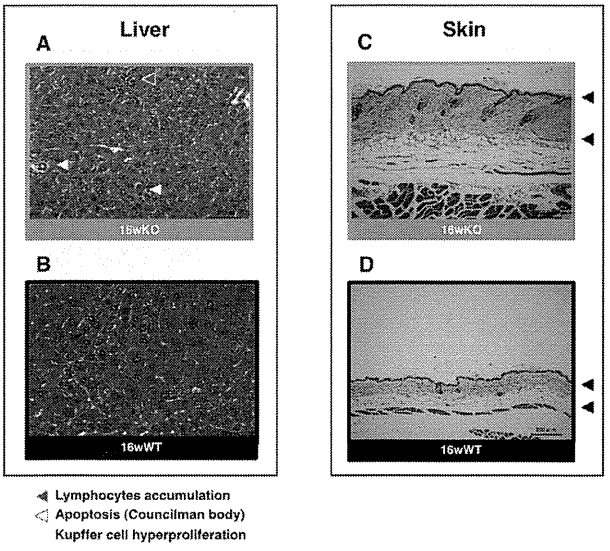

Figure 3. Inflammatory properties in the multiple organs of *TAX1BP1*-KO mice. The morphologic and functional alterations of the environments of liver (**A** and **B**) and skin (**C** and **D**) were also examined with HE-staining. Red and white triangles indicate accumulated lymphocytes and Councilman bodies respectively.
doi:10.1371/journal.pone.0073205.g003

Telemetric electrocardiogram (ECG)

Sixteen week old male *TAX1BP1*-KO or WT littermates with or without antibiotic treatment (n = 5/group) were monitored with telemetric electrocardiogram. Telemetric transmitter was implanted into the back of mice under aseptic conditions and the muscle layers and the skin were closed with resorbable sutures. Data were acquired at least 72 hour after the implantation with a receiver placed under the cage and a full-disclosure 72 hour recordings were analyzed off-line and the P-Q intervals were evaluated.

Antibiotic treatment

TAX1BP1-KO or WT littermate male mice were first raised with the normal diets and water for 4 weeks, and then, antibiotic group (n = 5/groups) received ampicillin (1 g/L; Wako), vancomycin hydrochloride (500 mg/L; Wako), neomycin trisulfate salt hydrate (1 g/L; Sigma-Aldrich), and metronidazole (1 g/L; Wako) in drinking water for 12 weeks [24]. The non-antibiotic controls were equally raised and maintained except for antibiotics treatment. Both groups of mice were maintained in flexible film isolators under a strict 12-hour light cycle and fed an autoclaved chow diet and tap water ad libitum. Germ free status was verified regularly by ensuring negative cultures from mouse feces in three media types: nutrient agar (Nissui), pourmedia sheep blood agar M70 (Eiken), and Sabouraud agar (Nissui). Microbial colonies were counted after incubation at 37°C for 48 hour (aerobes) or 72 hour (anaerobes). Both groups of mice were anesthetized and sacrificed at the end of 16 weeks experimental period. Daily fluid consumption, body weight, liver function (ALT, AST), renal

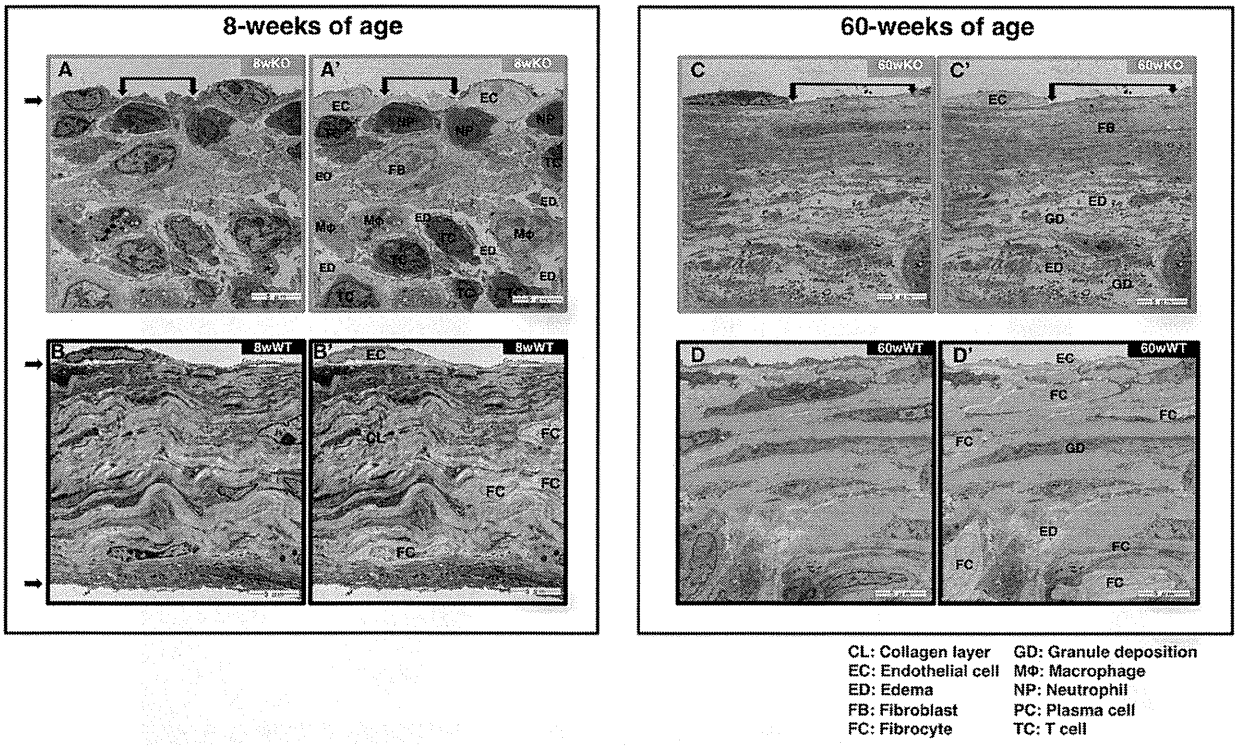

Figure 4. Massive infiltration of inflammatory cells causes severe tissue lesion in the mitral valves of *TAX1BP1*-KO mice. Electron microscopy examinations on the mitral valves of 8-, 16- and 60-wk *TAX1BP1*-KO mice (**A:** 8wKO, and **C:** 60wKO) and their WT littermates (**B:** 8wWT and **D:** 60wWT). See Figure S1 for details. Each panel was duplicated with colorized areas in specific cell types and abbreviated descriptions (Fig. 4A' to 4D'). Abbreviations, CL: Collagen layer; EC: Endothelial cell; ED: Edema; FB: Fibroblast; FC: Fibrocyte; GD: Granule deposition; MΦ: Macrophage; NP: Neutrophil; PC: Plasma cell; TC: T cell.
doi:10.1371/journal.pone.0073205.g004

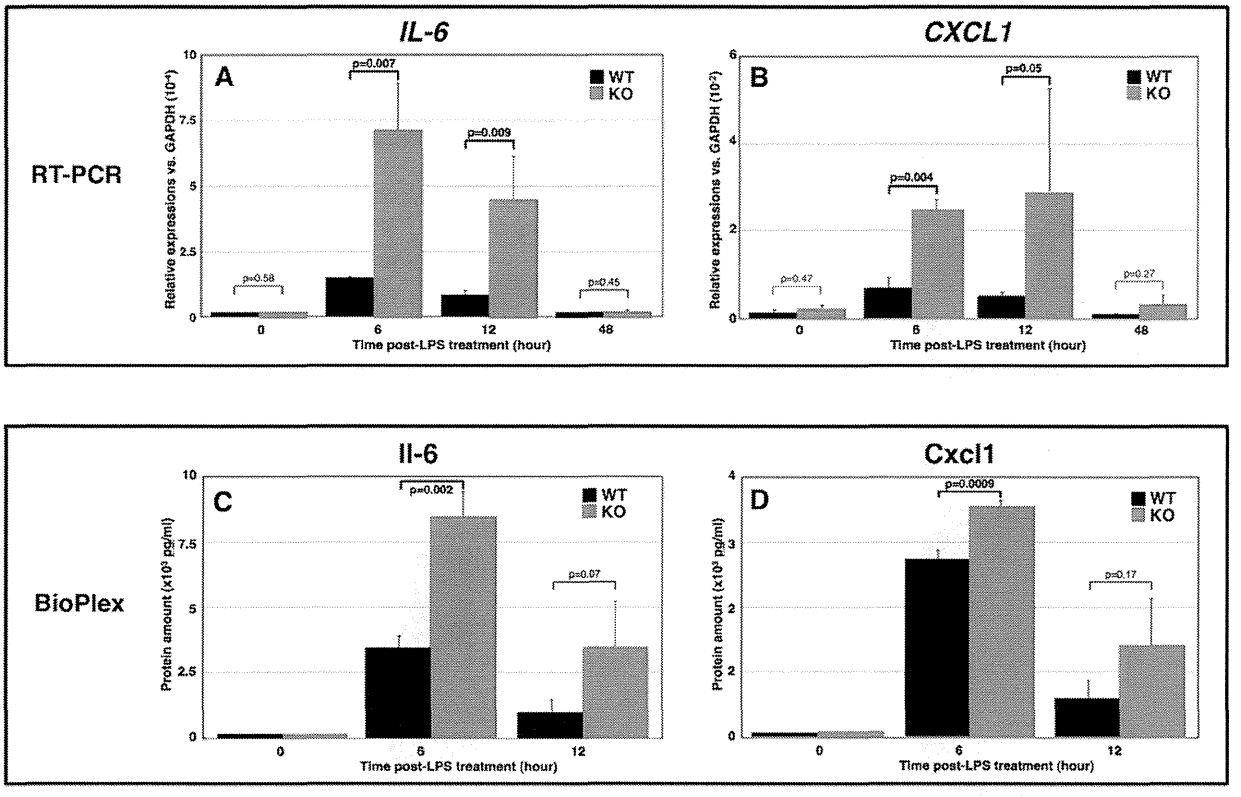

Figure 5. Enhanced expression of inflammatory genes after the LPS-stimulation to *TAX1BP1*-KO mice. 200 μg of *Salmonella typhimurium* lipopolysaccharide (LPS) in 100 μl sterile pyrogen-free saline were injected into a right footpads of *TAX1BP1*-KO or WT littermate mice. At the time 2, 6, 12, 24 and 48 hour post-injection (PT), each group of mouse were euthanized and tissues including serum, lymphocytes and eyes were collected. **A**) LPS-triggered induction of Tax1bp1 in eye tissue was monitored. Ten μg of cell lysates from WT BL6 mice at 2, 6, 12, 24 and 48 hour PT of LPS were probed with anti-Tax1bp1, -I-κBα and -Tubulin antibodies. **B, C**) Total RNAs of eye tissues from at 6, 12 and 48 hour PT of LPS to *TAX1BP1*-KO or WT littermates and their untreated controls were prepared and the expressions of *IL-6* and *CXCL1* were quantitated with RT-PCR. **D, E**) Sera from at 6, 12 and 48 hour PT of LPS to *TAX1BP1*-KO or WT littermates and their untreated controls were collected and the amount of Il-6 and Cxcl1 were quantitated with multiplex ELISA system (BioRad). Gray bar: *TAX1BP1*-KO, black bar: WT littermate.
doi:10.1371/journal.pone.0073205.g005

function (BUN), nutritional status (TG, GLU, TP) and spleen weight (After 10% formalin fixation) were examined. Caecum surface area was measured with Image J (NIH). In general, there were no particular adverse effects on mice through antibiotic treatment.

Statistical analysis

All numerical data are expressed as means ± SD. Statistical significance was assessed by Student's two-tailed t-test. In the case of ELISA, Statistical analyses were performed by one-way analysis of variance and Steel-Dwass test. Data were considered significant when $P<0.05$.

Results

LCM- and gene expression microarray array-based profiling of the mitral valves in *TAX1BP1*-KO mice and reevaluation by RT-PCR and immunostaining

We have previously observed that the mRNA expression level for several inflammatory cytokines, including IL-1β and TNFα, increases in the cardiac and skin tissues of *TAX1BP1*-KO mice; more importantly, these mice showed mitral valvulitis and premature death compared to their wild-type (WT) littermates. However, the underlying mechanisms involved in these processes remain unknown [8].

To date, information on variations in the levels of gene expression in regions of the heart (more specifically, the mitral valves) showing inflammation in *TAX1BP1*-KO mice is still lacking. This pathologic event is thought to be linked to premature death, which might be brought on by cardiac failure. In the current study, we employed LCM- and gene expression microarray-based techniques to obtain detailed information on the levels of gene expression in organs showing pathological changes. Total RNA was extracted from three independent tissue samples obtained from the mitral valves of 8- or 16- week-old (-wk) male (WT and TAX1BP1-KO) mice by using LCM, which was followed by total RNA extraction. Then, global mRNA expression profiles were analyzed by an Agilent gene expression microarray.

Principle component analysis, using two principle components, was conducted and the results were represented by a scatterplot (Fig. 1A). The data showed that the results for all samples from *TAX1BP1*-KO mice clearly deviated from those for control mice, indicating detectable differences in the gene transcription patterns of the two genetic backgrounds. A gene list was compiled on the basis of normalization and statistical analysis ($P<0.03$, logFC >1.0). Using these criteria, alterations in 588 gene expression profiles were identified. Unsupervised hierarchical clustering

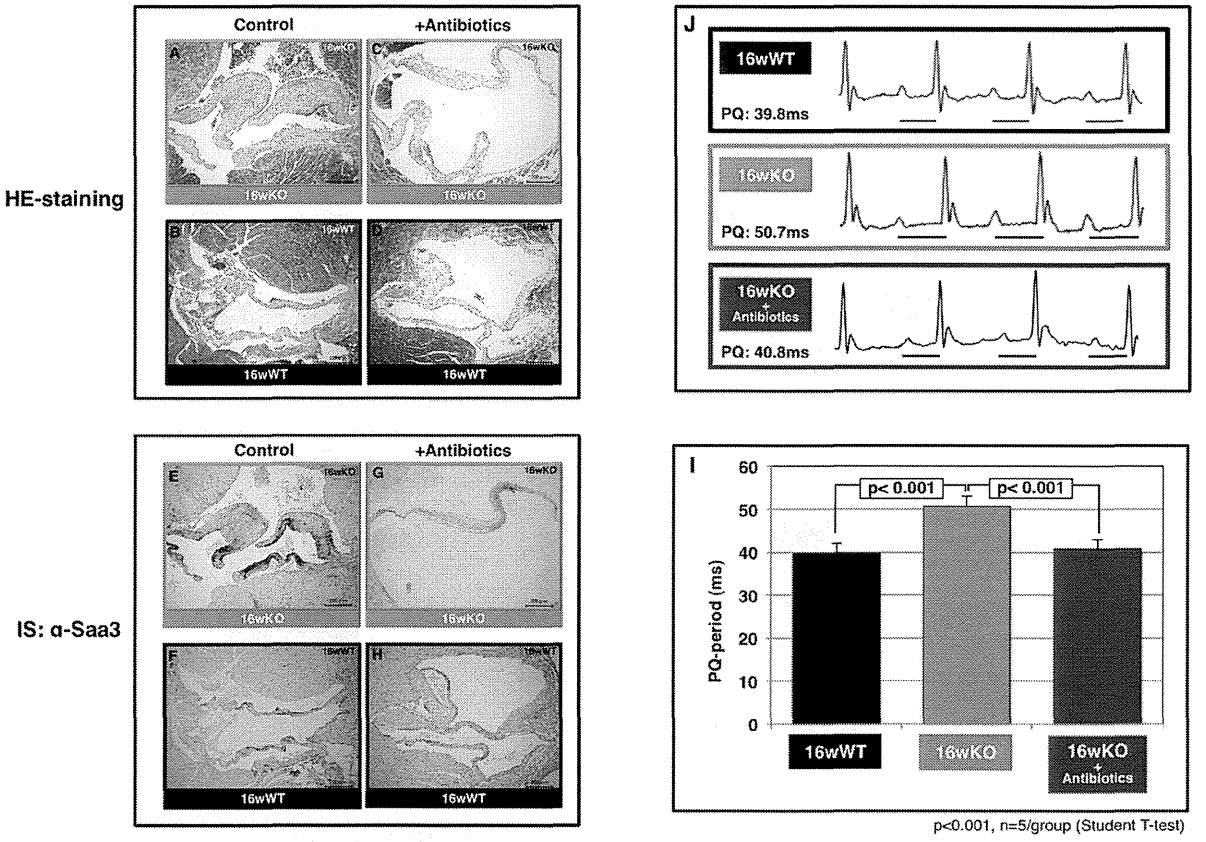

Figure 6. Amelioration of inflammatory valvulitis and conduction disturbance after the antibiotics treatment on *TAX1BP1*-KO mice. *TAX1BP1*-KO or WT littermate mice (male) were first raised with the normal diets and water for 4 weeks, and then, antibiotic treatment group (**C**, **D**, **G** and **H**, n = 5/group) provided ampicillin (1 g/L; Wako), vancomycin Hydrochloride (500 mg/L; Wako), neomycin trisulfate salt hydrate (1 g/L; Sigma-Aldrich), and metronidazole (1 g/L; Wako) in drinking water for 12 weeks based on a protocal of the commensal depletion (Rakoff-Nahoum S., Cell 2004). The non-antibiotics controls (**A**, **B**, **E** and **F**, n = 5/group) were equally raised and maintained except for antibiotics treatment. Each group of mice were anesthetized and sacrificed at the end of 16 weeks experimental period and histochemical representatives of each group were displayed with HE-staining (**A** to **D**) or anti-Saa3 immuno-staining (IS, **E** to **H**). **I**). Heart rhythms of 16-week-old *TAX1BP1*-KO treated with antibiotics over 12 weeks (male, n = 5/group) were monitored with telemetric electrocardiogram (12-lead ECG). **J**) The average values of PQ-intervals were compared with those of untreated *TAX1BP1*-KO mice and their WT littermates.
doi:10.1371/journal.pone.0073205.g006

analysis (Cluster 3.0; Stanford University) of the 588 genes resulted in the separation of all *TAX1BP1*-KO from their paired WT controls. In total, 428 probes were upregulated and 160 were downregulated for a total of 24,000 genes (Fig. 1B). We then applied volcano plot analysis to identify the differences in mitral valve mRNA expression in *TAX1BP1*-KO mice and the controls.

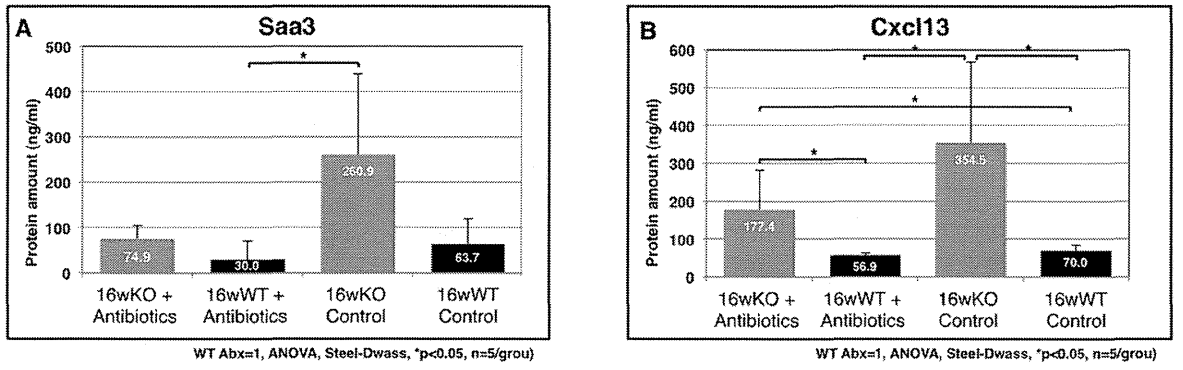

Figure 7. Reduction of the Saa3 and Cxcl1 expression in the sera of TAX1BP1-KO mice after the antibiotics treatment. ELISA quantitation of Saa3 (**A**) or Cxcl13 (**B**) of the sera on four groups were performed. Gray bar: *TAX1BP1*-KO mice, black bar: WT littermates (n = 5/group).
doi:10.1371/journal.pone.0073205.g007

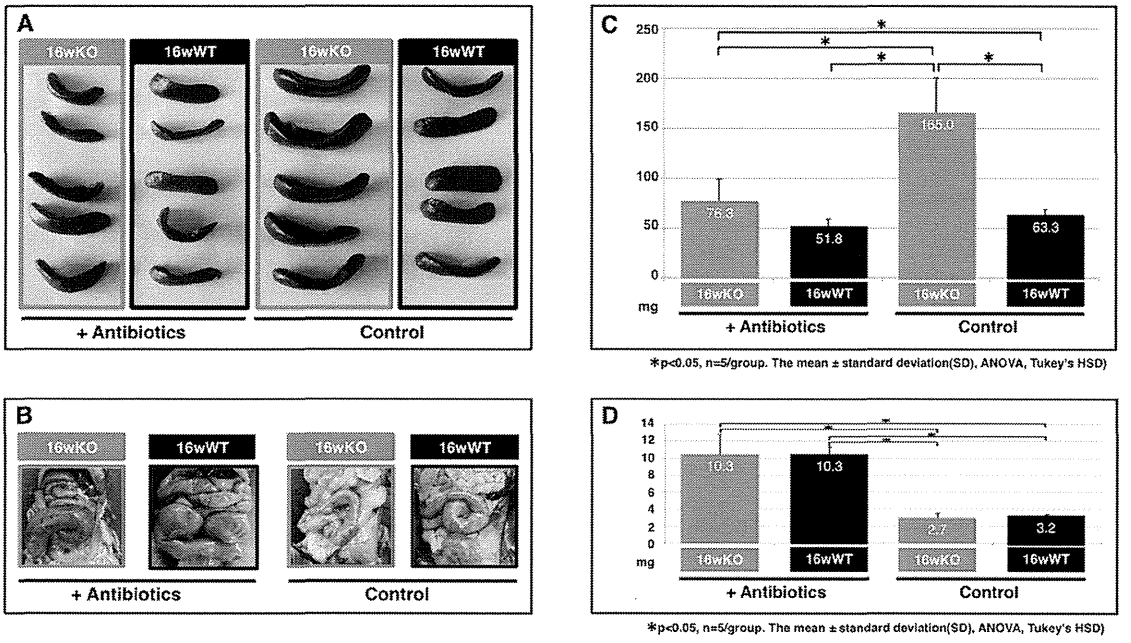

Figure 8. Splenic hypertrophy of *TAX1BP1*-KO mice and its cancellation by antibiotics treatment. Examinations on the spleen volume (**A**) and the area of cecum (**B**) were performed. The average values of spleen volumes (**C**) and cecum areas (**D**) were displayed (n = 5/group).
doi:10.1371/journal.pone.0073205.g008

The plot showed a log2-fold change in mRNA expression between the two groups on the x-axis and the negative log of the t-test p-values on the y-axis. Each gene was represented by a single dot. Using the plot, we identified 588 probes that showed a more than 2-fold differential expression of mRNA when compared to the controls ($p<0.03$, Fig. 1C).

Tables 3 and 4 list the gene symbols, gene descriptions, fold changes, and p-value for all genes upregulated by more than 20-

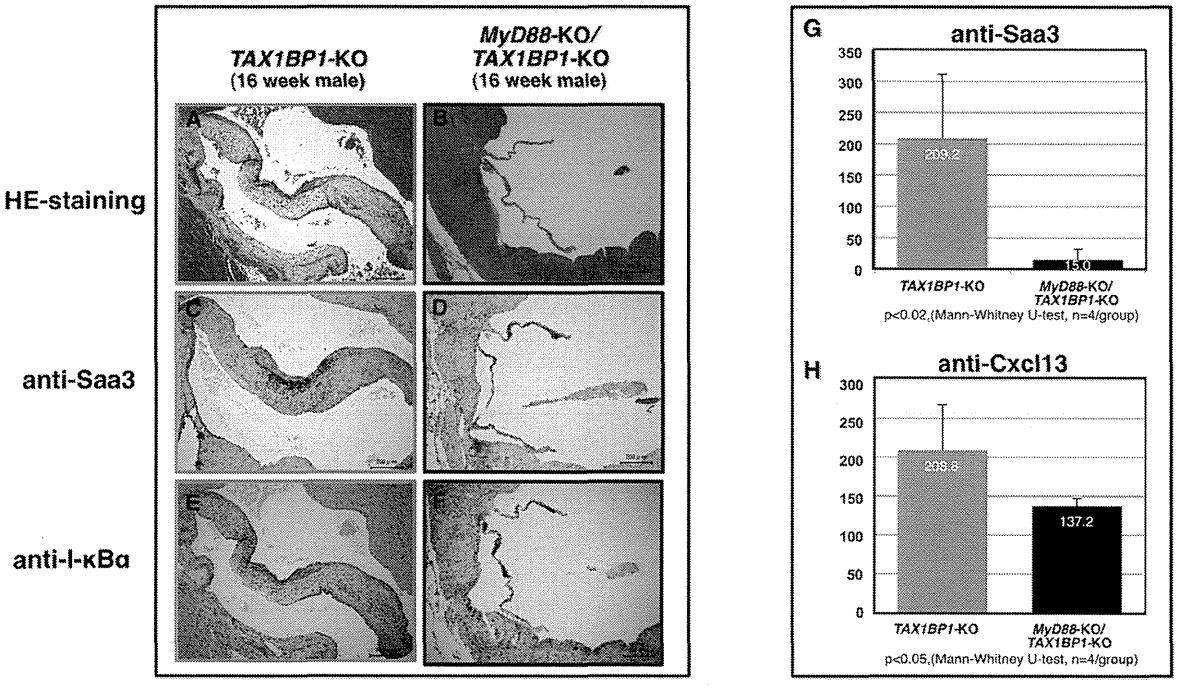

Figure 9. Cancelation of valvulitis in the *MyD88/TAX1BP1* double-KO mice. The HE-staining (A, B) and immunostaining of Saa3 (C, D) and I-κBα (E, F) were compared between *TAX1BP1*-KO and *MyD88/TAX1BP1*-KO mice. ELISA quantification of Saa3 (I) and Cxcl13 on the sera of both genetic background.
doi:10.1371/journal.pone.0073205.g009

fold or downregulated by more than 5-fold. Most of the upregulated genes were primarily involved in inflammation. The gene showing the highest level of induction, *SAA3*, (i.e., 1,180 fold induction) along with *SAA1* (i.e., 61 fold, 10th induction) are well-known inflammatory markers in patients with autoimmune disease, chronic infection and cancer [25]. *SAA3* is also hyper-induced at the site of injury [26], inflammation [27] in mice experimental models. Additionally, genes related to immune modulation, including pathogen recognition, inflammation, chemotaxis [28–30], or tissue adhesion, degeneration and rearrangement [31,32] were induced in the mitral valves of *TAX1BP1*-KO mice. The characteristics of the downregulated genes also suggested the link between inflammation and tissue degeneration (Table S1); for example, such as *WIF1*, a Wnt signaling suppressor; *UCMA*, a gene associated with cartilage development [33–35]. *EFCAB2* is a functional partner of the voltage-gated Ca^{2+} channel [36]. *TSC22D3* (also known as *GILZ*: a *G*lucocorticoid *I*nduced *L*eucine *Z*ipper) is an IL-10-inducible immune suppressor [37].

We further confirmed the microarray results for *SAA3* and *EFCAB2* by using RT-PCR (Fig. 2AB and Figure S1) and for Saa3 (induction) or I-κBα (reduction) by using immunostaining for mitral valve samples from 16-wk *TAX1BP1*-KO mice (Fig. 2C to F). In addition to these microenvironmental changes, broad-spectrum inflammatory effects, such as lymphocyte accumulation, apoptotic Councilman body formation, and Kupffer cell hyper proliferation in the hepatocyte (Fig. 3A), and thickening of the inflamed skin (Fig. 3C), were observed in 16-wk *TAX1BP1*-KO mice. Multiplex ELISA quantitation of the sera for homozygous or heterozygous *TAX1BP1*-KO and their WT littermates showed age-dependent development of systemic inflammation (Table S1). The levels of Il-6 and Cxcl1 were elevated more than 10- fold in the homozygous *TAX1BP1*-KO mice.

Massive infiltration of inflammatory lymphocytes in the mitral valves of *TAX1BP1*-KO mice

To obtain more detailed images of critical sites of inflammation, tissues obtained from the mitral valves of *TAX1BP1*-KO mice and their WT littermates at varying time points were examined with electron microscopy (Fig. 4). Surprisingly, the mitral valves *TAX1BP1*-KO mice showed extensive infiltration of lymphocytes, macrophages and neutrophils and tissue degeneration at only 8 weeks of age (Fig. 4A and 4A'), whereas the mitral valves of the WT littermates exhibited healthy collagen layers (Fig. 4B and 4B'). Extensive disruption of collagen layers and edema were observed at 60 weeks of age for *TAX1BP1*-KO mice (Fig. 4C, 4D and 4C', 4D').

Enhanced inflammatory responses in *TAX1BP1*-KO mice after the LPS-stimulation

In addition to the chronic inflammation, the acute-phase inflammatory response of *TAX1BP1*-KO mice was also examined. *Salmonella typhimurium* lipopolysaccharide (LPS) was injected into the footpads of *TAX1BP1*-KO mice and their WT littermates. Then, the mice were monitored, and the effects were recorded. We examined the kinetics of mRNA expression in those same eye tissues (Fig. 5A, B: tissue specific) and the translational products in the sera (Fig. 5C, D: systemic) of *IL-6* and *CXCL1* were monitored. Both data clearly indicate that a deficiency in *TAX1BP1* causes significantly enhanced inflammation in responses to LPS in *TAX1BP1*-KO mice.

Amelioration of the inflammatory symptoms and the cardiac conduction defect of *TAX1BP1*-KO mice by antibiotic treatment and simultaneous *MyD88* deficiency

Microbial infections spontaneously cause severe endothelial inflammatory diseases such as rheumatic fever and Kawasaki disease [38]. At the subcellular level, modulation of the threshold of immune cell activation, differentiation, and immune cell activity in response to non-self or self antigens in *TAX1BP1*-KO mice (Fig. 1 and Tables 3 and 4) might evoke autoimmune profiles and heart dysfunction. To test this hypothesis, we examined the link between the commensal microbiota and mitral valvulitis and endocarditis in *TAX1BP1*-KO mice. When the mice were 4 weeks old, antibiotics were orally administered to all subjects over a 12-week period. The telemetric electrocardiogram profiles then sacrificed for the pathologic examination. Inflammatory hypertrophy (Fig. 6A) and extensive Saa3 staining (Fig. 6E) of the mitral valves in *TAX1BP1*-KO mice were abolished with antibiotic treatments (Fig. 6C and G); no changes were observed in their WT littermates (Fig. 6B, D, F and H). Extended PQ-intervals observed by telemetric electrocardiogram in *TAX1BP1*-KO mice (Fig. 6I, middle panel) were alleviated with the administration of antibiotics (Fig. 6I, bottom panel). The statistical significance of the differences in the PQ-intervals was tested (Fig. 6J). The antibiotic regimen also reduced the secretion of Saa3 and Cxcl13 in the sera of *TAX1BP1*-KO mice (Fig. 7A, B), and splenic hypertrophy of *TAX1BP1*-KO mice was almost nonexistent (Fig. 8A). Typical cecum thickening due to antibiotic treatment was also confirmed (Fig. 8B), and fecal microbes were completely disappeared under these conditions (data not shown). If the eradication of microbiota is the main reason for the amelioration of the symptoms in *TAX1BP1*-KO mice, we hypothesized that the disruption of the innate immune cascade could bring about similar results. We crossbred *TAX1BP1*-KO mice with *MyD88*-KO mice [20] and examined the morphological features or immunostaining profiles of marker proteins in the mitral valves of 16-week-old *TAX1BP1*-KO and *MyD88/TAX1BP1*-KO mice. *MyD88/TAX1BP1*-double knockout canceled hyperplasia (Fig. 9A, B), Saa3 induction (Fig. 9C, D) and I-κBα degradation (Fig. 9E, F). Comparisons of ELISA values for *TAX1BP1*-KO and *MyD88/TAX1BP1*-KO mice also indicated amelioration of the inflammatory response in *MyD88/TAX1BP1*-KO mice (Fig. 9G, H).

Discussion

Chronic infection with a retrovirus can have a significant impact on the host immune system. In the case of HTLV-1 infection, the pathological features of the disease are influenced by multiple factors. While HIV causes immune deficiency in the host, HTLV-1 causes a wide range of inflammatory symptoms (HAM and HU) and, in some cases, immunosuppressive ATL, a malignant growth of regulatory T-lymphocytes [39,40]. Furthermore, HAD patients frequently display impaired immune response such as an ineffective interferon response in HAM patients [41] and frequent development of dermatitis in ATL patients [42].

Multiple inflammatory symptoms, including cardiac valvulitis, dermatitis, and a hypersensitive response to endotoxins and inflammatory cytokines, were noted in our preclinical model involving *TAX1BP1-KO* mice. More importantly, *TAX1BP1-KO* mice died prematurely because of unknown mechanisms [8]. In this study, we discovered the hyper-induction of multiple inflammation-related genes including *SAA3*, *CHI3L1*, *HP*, *IL1B*, *SPP1/OPN*, and the significant reduction of *TSC22D3/GILZ* in the mitral valves and microenvironment deterioration in a progressive age-dependent manner for *TAX1BP1*-KO mice [43–47], the

significant reduction of *EFCAB2* expression was highly implicated in functional defects of the heart [36].

HTLV-1-transgenic mice develop autoimmune symptom closely related to those observed for rheumatoid arthritis [48] or Sjögren's syndrome [49]. A rat model, infected with the HTLV-1 producing cell line, is known to develop HAM-like myelopathies in seronegative carrier rats [50]. A Tax1-transgenic mouse model, which specifically expresses Tax1 in T-lymphocytes, illustrates the development of aggressive ATL-like lymphoma with continuous invasion of lymphomatous cells into multiple organs such as the skin, liver and spleen [51,52]. Subcutaneous inoculation of HTLV-1 transformed cells into NOG mice also results in ATL-like symptoms [53]. These transgenic/transplant models show symptoms similar to those found in human clinical cases. Furthermore, HTLV-1-driven inflammatory symptoms tend to occur in patients with HAD under normal host immune response conditions, while ATL-like symptoms develop under immunosuppressive conditions [54].

TAX1BP1-KO mice displayed invasive growth of lymphocytes into multiple organs (Fig. 3) and splenic hypertrophy (Fig. 8). We previously observed that transplantation of *TAX1BP1*-KO bone marrow to γ-irradiated normal mice resulted in the same inflammatory responses [8]. These results imply that *TAX1BP1*-KO model may be correlated with inflammatory HAD. The novelty of this system is identification of possible risk factors associated with vascular disease in HTLV-1 carriers [17,18]. Preliminary electrocardiogram experiments using *TAX1BP1*-KO mice showed an abnormal prolongation of PQ intervals and/or atrioventricular conduction defects (Fig. 6I, J), which might cause fatal cardiac failure. Since the PQ interval and atrioventricular conduction highly depend on the functioning of voltage-dependent L-type Ca^{2+} channels, L-type Ca^{2+} channel function may deteriorate in the heart of *TAX1BP1*-KO mice. Of note, *EFCAB2*, a functional partner in the voltage-gated Ca^{2+} channel, was significantly downregulated in the cardiac tissue of *TAX1BP1*-KO mice (Table 4). Further studies are required to elucidate these defects caused in *TAX1BP1*-KO mice.

Intensive antibiotic treatment [24] for *TAX1BP1*-KO mice significantly ameliorated inflammatory symptoms (Fig. 6). *TAX1BP1*-KO mice crossbred with *MyD88*-KO mice showed similar results. Since the intrinsic role of Tax1bp1 is to inhibit unnecessarily activated innate immunity responses [8], a functional deficiency of Tax1bp1 through HTLV-1 infection can lead to similar symptoms in humans; that is, commensal microbiota can cause pseudo-Infective endocarditis symptoms [55]. The extent of the deficiency, however, is much more moderate than that of typical infective endocarditis (IE) [56].

A large population-based epidemiological study revealed that the prevalence of heart valve disease in the entire population of the United States is 2.5% [53]. IE is thought to result from the following sequence of events: (1) the formation of nonbacterial thrombotic endocarditis on the surface of a cardiac valve or elsewhere that endothelial damage occurs; (2) bacteremia; and (3) the adherence of the bacteria in the bloodstream to nonbacterial thrombotic endocarditis and proliferation of bacteria within a vegetation [57]. Viridans group streptococci are a part of normal skin, oral, respiratory, and gastrointestinal tract flora, and are responsible for ≥50% of community-acquired native valve IE cases [58]. Another review reported that 20% of IE cases originated from culture-negative or Enterococci [59]. Each of these epidemiological surveys clearly indicates the importance of prevention and control measures with regard to microbial infection and vegetation. However, it is still not known why IE is developed in limited population and it is not clear whether there are any differences in the frequencies of allelic polymorphisms in the immune response genes for IE patients?

In summary, HTLV-1 induces diverse forms of inflammatory disorders [60,61], which may originate from the functional dysregulation of Tax1bp1. Single-nucleotide polymorphisms (SNPs) in *A20* or *RNF11*, catalytic partners of Tax1bp1, has have linked to many inflammatory diseases [19,62,63]. However, in the case of *TAX1BP1* SNPs, only one study has linked them to the head and neck cancer [64]. The genetic variations in *TAX1BP1* and its partners would provide novel insights on the pathogenic machinery of HADs.

Supporting Information

Figure S1 Validation of genes identified their expression alteration in the mitral valves of TAX1BP1-KO mice. RT-PCR validation of genes identified their expression alteration in the mitral valves of *TAX1BP1*-KO mice, **A**) *CCL2* **B**) *CHI3L1* respectively. Gray bar: *TAX1BP1*-KO, black bar: WT. Mitral valve specimens were prepared as described in Fig. 2A. Primers and probes were as indicated.
(PDF)

Table S1 Age-dependent induction of pro-inflammatory proteins in the sera of *TAX1BP1*-KO mice. Sera from four different weeks of age (3, 8, 16 and 32) of *TAX1BP1* homozygous knockout (Homo-KO), heterozygous knockout (Hetero-KO) or their WT littermates were collected and examined with multiplex ELISA quantitation kit (Bio-Plex Pro™ Mouse Cytokine 23-plex Assay, BioRad). Each value is an average of four different samples.
(PDF)

Acknowledgments

This paper is dedicated for the memories of the late Dr. Kuan-Teh Jeang who passed away on January 27th, 2013.

Author Contributions

Conceived and designed the experiments: HI KO AN. Performed the experiments: SN EI YT YW T. Matsumoto T. Mitsui TY K. Inoue HK AY K. Ito TS HI. Contributed reagents/materials/analysis tools: SY NT KTJ MH MM TK. Wrote the paper: SN KTJ KO AN HI. Conducted bioinformatics: SN YT WF HI.

References

1. Newton K, Dixit VM (2012) Signaling in innate immunity and inflammation. Cold Spring Harb Perspect Biol 4.
2. McCool KW, Miyamoto S (2012) DNA damage-dependent NF-kappaB activation: NEMO turns nuclear signaling inside out. Immunol Rev 246: 311–326.
3. Hayden MS, Ghosh S (2012) NF-kappaB, the first quarter-century: remarkable progress and outstanding questions. Genes Dev 26: 203–234.
4. DiDonato JA, Mercurio F, Karin M (2012) NF-kappaB and the link between inflammation and cancer. Immunol Rev 246: 379–400.
5. Verstrepen L, Verhelst K, van Loo G, Carpentier I, Ley SC, et al. (2010) Expression, biological activities and mechanisms of action of A20 (TNFAIP3). Biochem Pharmacol 80: 2009–2020.
6. Shembade N, Harhaj EW (2012) Regulation of NF-kappaB signaling by the A20 deubiquitinase. Cell Mol Immunol 9: 123–130.
7. De Valck D, Jin DY, Heyninck K, Van de Craen M, Contreras R, et al. (1999) The zinc finger protein A20 interacts with a novel anti-apoptotic protein which is cleaved by specific caspases. Oncogene 18: 4182–4190.
8. Iha H, Peloponese JM, Verstrepen L, Zapart G, Ikeda F, et al. (2008) Inflammatory cardiac valvulitis in TAX1BP1-deficient mice through selective NF-kappaB activation. EMBO J 27: 629–641.

9. Shembade N, Harhaj NS, Liebl DJ, Harhaj EW (2007) Essential role for TAX1BP1 in the termination of TNF-alpha-, IL-1- and LPS-mediated NF-kappaB and JNK signaling. EMBO J 26: 3910–3922.
10. Ling L, Goeddel DV (2000) T6BP, a TRAF6-interacting protein involved in IL-1 signaling. Proc Natl Acad Sci U S A 97: 9567–9572.
11. Peloponese JM, Yeung ML, Jeang KT (2006) Modulation of nuclear factor-kappaB by human T cell leukemia virus type 1 Tax protein: implications for oncogenesis and inflammation. Immunol Res 34: 1–12.
12. Giam CZ, Jeang KT (2007) HTLV-1 Tax and adult T-cell leukemia. Front Biosci 12: 1496–1507.
13. Shembade N, Harhaj NS, Parvatiyar K, Copeland NG, Jenkins NA, et al. (2008) The E3 ligase Itch negatively regulates inflammatory signaling pathways by controlling the function of the ubiquitin-editing enzyme A20. Nat Immunol 9: 254–262.
14. Verstrepen L, Verhelst K, Carpentier I, Beyaert R (2011) TAX1BP1, a ubiquitin-binding adaptor protein in innate immunity and beyond. Trends Biochem Sci 36: 347–354.
15. Yamaoka S, Courtois G, Bessia C, Whiteside ST, Weil R, et al. (1998) Complementation cloning of NEMO, a component of the IkappaB kinase complex essential for NF-kappaB activation. Cell 93: 1231–1240.
16. Hida A, Imaizumi M, Sera N, Akahoshi M, Soda M, et al. (2010) Association of human T lymphotropic virus type I with Sjogren syndrome. Ann Rheum Dis 69: 2056–2057.
17. Kira J, Hamada T, Kawano Y, Okayama M, Yamasaki K (1997) An association of human T-cell lymphotropic virus type I infection with vascular dementia. Acta Neurol Scand 96: 305–309.
18. Hayashi J, Furusyo N, Sawayama Y, Murata M (2008) [Chronic infection is one of the etiologies for digestive diseases and atherosclerosis]. Fukuoka Igaku Zasshi 99: 67–73.
19. Vereecke L, Beyaert R, van Loo G (2009) The ubiquitin-editing enzyme A20 (TNFAIP3) is a central regulator of immunopathology. Trends Immunol 30: 383–391.
20. Kawai T, Adachi O, Ogawa T, Takeda K, Akira S (1999) Unresponsiveness of MyD88-deficient mice to endotoxin. Immunity 11: 115–122.
21. Sadanaga A, Nakashima H, Akahoshi M, Masutani K, Miyake K, et al. (2007) Protection against autoimmune nephritis in MyD88-deficient MRL/lpr mice. Arthritis Rheum 56: 1618–1628.
22. Benjamini Y, Drai D, Elmer G, Kafkafi N, Golani I (2001) Controlling the false discovery rate in behavior genetics research. Behav Brain Res 125: 279–284.
23. Iha H, Kibler KV, Yedavalli VR, Peloponese JM, Haller K, et al. (2003) Segregation of NF-kappaB activation through NEMO/IKKgamma by Tax and TNFalpha: implications for stimulus-specific interruption of oncogenic signaling. Oncogene 22: 8912–8923.
24. Rakoff-Nahoum S, Paglino J, Eslami-Varzaneh F, Edberg S, Medzhitov R (2004) Recognition of commensal microflora by toll-like receptors is required for intestinal homeostasis. Cell 118: 229–241.
25. Obici L, Merlini G (2012) Amyloidosis in autoinflammatory syndromes. Autoimmun Rev 12: 14–17.
26. Jang SY, Shin YK, Lee HY, Park JY, Suh DJ, et al. (2012) Local production of serum amyloid a is implicated in the induction of macrophage chemoattractants in Schwann cells during wallerian degeneration of peripheral nerves. Glia 60: 1619–1628.
27. Poynter ME (2012) Airway epithelial regulation of allergic sensitization in asthma. Pulm Pharmacol Ther 25: 438–446.
28. Geijtenbeek TB, Gringhuis SI (2009) Signalling through C-type lectin receptors: shaping immune responses. Nat Rev Immunol 9: 465–479.
29. Kapoor M, Martel-Pelletier J, Lajeunesse D, Pelletier JP, Fahmi H (2011) Role of proinflammatory cytokines in the pathophysiology of osteoarthritis. Nat Rev Rheumatol 7: 33–42.
30. Goldszmid RS, Trinchieri G (2012) The price of immunity. Nat Immunol 13: 932–938.
31. Lee CG, Da Silva CA, Dela Cruz CS, Ahangari F, Ma B, et al. (2011) Role of chitin and chitinase/chitinase-like proteins in inflammation, tissue remodeling, and injury. Annu Rev Physiol 73: 479–501.
32. Das R, Philip S, Mahabeleshwar GH, Bulbule A, Kundu GC (2005) Osteopontin: it's role in regulation of cell motility and nuclear factor kappa B-mediated urokinase type plasminogen activator expression. IUBMB Life 57: 441–447.
33. Gudjonsson JE, Johnston A, Stoll SW, Riblett MB, Xing X, et al. (2010) Evidence for altered Wnt signaling in psoriatic skin. J Invest Dermatol 130: 1849–1859.
34. Chien AJ, Conrad WH, Moon RT (2009) A Wnt survival guide: from flies to human disease. J Invest Dermatol 129: 1614–1627.
35. Surmann-Schmitt C, Dietz U, Kireva T, Adam N, Park J, et al. (2008) Ucma, a novel secreted cartilage-specific protein with implications in osteogenesis. J Biol Chem 283: 7082–7093.
36. Heineke J, Auger-Messier M, Correll RN, Xu J, Benard MJ, et al. (2010) CIB1 is a regulator of pathological cardiac hypertrophy. Nat Med 16: 872–879.
37. Berrebi D, Bruscoli S, Cohen N, Foussat A, Migliorati G, et al. (2003) Synthesis of glucocorticoid-induced leucine zipper (GILZ) by macrophages: an anti-inflammatory and immunosuppressive mechanism shared by glucocorticoids and IL-10. Blood 101: 729–738.
38. Wilson W, Taubert KA, Gewitz M, Lockhart PB, Baddour LM, et al. (2008) Prevention of infective endocarditis: guidelines from the American Heart Association: a guideline from the American Heart Association Rheumatic Fever, Endocarditis and Kawasaki Disease Committee, Council on Cardiovascular Disease in the Young, and the Council on Clinical Cardiology, Council on Cardiovascular Surgery and Anesthesia, and the Quality of Care and Outcomes Research Interdisciplinary Working Group. J Am Dent Assoc 139 Suppl: 3S–24S.
39. Sandler NG, Douek DC (2012) Microbial translocation in HIV infection: causes, consequences and treatment opportunities. Nat Rev Microbiol 10: 655–666.
40. Tattermusch S, Bangham CR (2012) HTLV-1 infection: what determines the risk of inflammatory disease? Trends Microbiol 20: 494–500.
41. Martin F, Taylor GP (2011) Prospects for the management of human T-cell lymphotropic virus type 1-associated myelopathy. AIDS Rev 13: 161–170.
42. Yagi H, Takigawa M, Hashizume H (2003) Cutaneous type of adult T cell leukemia/lymphoma: a new entity among cutaneous lymphomas. J Dermatol 30: 641–643.
43. Uhlar CM, Whitehead AS (1999) Serum amyloid A, the major vertebrate acute-phase reactant. Eur J Biochem 265: 501–523.
44. Elias JA, Homer RJ, Hamid Q, Lee CG (2005) Chitinases and chitinase-like proteins in T(H)2 inflammation and asthma. J Allergy Clin Immunol 116: 497–500.
45. Quaye IK (2008) Haptoglobin, inflammation and disease. Trans R Soc Trop Med Hyg 102: 735–742.
46. Dinarello CA (2009) Immunological and inflammatory functions of the interleukin-1 family. Annu Rev Immunol 27: 519–550.
47. Uede T (2011) Osteopontin, intrinsic tissue regulator of intractable inflammatory diseases. Pathol Int 61: 265–280.
48. Iwakura Y, Tosu M, Yoshida E, Takiguchi M, Sato K, et al. (1991) Induction of inflammatory arthropathy resembling rheumatoid arthritis in mice transgenic for HTLV-I. Science 253: 1026–1028.
49. Green JE, Hinrichs SH, Vogel J, Jay G (1989) Exocrinopathy resembling Sjogren's syndrome in HTLV-1 tax transgenic mice. Nature 341: 72–74.
50. Ishiguro N, Abe M, Seto K, Sakurai H, Ikeda H, et al. (1992) A rat model of human T lymphocyte virus type I (HTLV-I) infection. 1. Humoral antibody response, provirus integration, and HTLV-I-associated myelopathy/tropical spastic paraparesis-like myelopathy in seronegative HTLV-I carrier rats. J Exp Med 176: 981–989.
51. Hasegawa H, Sawa H, Lewis MJ, Orba Y, Sheehy N, et al. (2006) Thymus-derived leukemia-lymphoma in mice transgenic for the Tax gene of human T-lymphotropic virus type I. Nat Med 12: 466–472.
52. Ohsugi T, Kumasaka T, Okada S, Urano T (2007) The Tax protein of HTLV-1 promotes oncogenesis in not only immature T cells but also mature T cells. Nat Med 13: 527–528.
53. Dewan MZ, Terashima K, Taruishi M, Hasegawa H, Ito M, et al. (2003) Rapid tumor formation of human T-cell leukemia virus type 1-infected cell lines in novel NOD-SCID/gammac(null) mice: suppression by an inhibitor against NF-kappaB. J Virol 77: 5286–5294.
54. Chervonsky AV (2010) Influence of microbial environment on autoimmunity. Nat Immunol 11: 28–35.
55. Gould FK, Denning DW, Elliott TS, Foweraker J, Perry JD, et al. (2012) Guidelines for the diagnosis and antibiotic treatment of endocarditis in adults: a report of the Working Party of the British Society for Antimicrobial Chemotherapy. J Antimicrob Chemother 67: 269–289.
56. Seckeler MD, Hoke TR (2011) The worldwide epidemiology of acute rheumatic fever and rheumatic heart disease. Clin Epidemiol 3: 67–84.
57. Chu VH, Woods CW, Miro JM, Hoen B, Cabell CH, et al. (2008) Emergence of coagulase-negative staphylococci as a cause of native valve endocarditis. Clin Infect Dis 46: 232–242.
58. Moreillon P, Que YA (2004) Infective endocarditis. Lancet 363: 139–149.
59. Oliere S, Douville R, Sze A, Belgnaoui SM, Hiscott J (2011) Modulation of innate immune responses during human T-cell leukemia virus (HTLV-1) pathogenesis. Cytokine Growth Factor Rev 22: 197–210.
60. Roufosse FE, Goldman M, Cogan E (2007) Hypereosinophilic syndromes. Orphanet J Rare Dis 2: 37.
61. Musone SL, Taylor KE, Lu TT, Nititham J, Ferreira RC, et al. (2008) Multiple polymorphisms in the TNFAIP3 region are independently associated with systemic lupus erythematosus. Nat Genet 40: 1062–1064.
62. Matmati M, Jacques P, Maelfait J, Verheugen E, Kool M, et al. (2011) A20 (TNFAIP3) deficiency in myeloid cells triggers erosive polyarthritis resembling rheumatoid arthritis. Nat Genet 43: 908–912.
63. Sartelet A, Druet T, Michaux C, Fasquelle C, Geron S, et al. (2012) A splice site variant in the bovine RNF11 gene compromises growth and regulation of the inflammatory response. PLoS Genet 8: e1002581.
64. Ruiz MT, Balachi JF, Fernandes RA, Galbiatti AL, Maniglia JV, et al. (2010) Analysis of the TAX1BP1 gene in head and neck cancer patients. Braz J Otorhinolaryngol 76: 193–198.